# Endothelial cell signature in muscle stem cells validated by VEGFA-FLT1-AKT1 axis promoting survival of muscle stem cell

Authors/Affiliations

Mayank Verma[a,b,c,d], Yoko Asakura[b,c,d], Xuerui Wang[b,c,d], Kasey Zhou[b,c,d], Mahmut Ünverdi[b,c,d], Allison P. Kann[e,f], Robert S. Krauss[e,f] and Atsushi Asakura[b,c,d]

Department of Pediatrics & Neurology, Division of Pediatric Neurology, The University of Texas Southwestern Medical Center, TX, USA[a].

Stem Cell Institute[b], Paul & Sheila Wellstone Muscular Dystrophy Center[c], Department of Neurology[d], University of Minnesota Medical School, MN, USA

Department of Cell, Developmental, and Regenerative Biology[e], and Graduate School of Biomedical Sciences[f], Icahn School of Medicine at Mount Sinai, NY, USA.

Conflict of Interest

MV and AA are listed as inventors on a patent for anti-FLT1 antibody mediated therapy for DMD. AA received consulting fees from ShireHGT.

**Abstract**

Endothelial and skeletal muscle lineages arise from common embryonic progenitors. Despite their shared developmental origin, adult endothelial cells (ECs) and muscle stem cells (MuSCs) (satellite cells) have been thought to possess distinct gene signatures and signaling pathways. Here we shift this paradigm by uncovering how adult MuSC behavior is affected by the expression of a subset of EC transcripts. We used several computational analyses including single-cell RNAseq to show that MuSCs express low levels of canonical EC markers. We demonstrate that MuSC survival is regulated by one such prototypic endothelial signaling pathway (VEGFA-FLT1). Using pharmacological and genetic gain- and loss-of-function studies, we identify the FLT1-AKT1 axis as the key effector underlying VEGFA-mediated regulation of MuSC survival. All together, our data support that the VEGFA-FLT1-AKT1 pathway promotes MuSC survival during muscle regeneration, and highlights how the minor expression of select transcripts is sufficient for affecting cell behavior.

36 **Introduction**

37 Skeletal muscle and endothelial cells (ECs) and their progenitors from the trunk and limbs are
38 derived from the somites during early developments. Previous works demonstrated the existence
39 of bipotent progenitors which express both Pax3 and FLK1 (Eichmann et al., 1993; Ema et al.,
40 2006; Esner et al., 2006; Kardon et al., 2002; Tozer et al., 2007). These bipotent progenitors
41 migrate into trunk and limb buds from ventrolateral region of the somites to generate MyoD(+)
42 myogenic cells followed by skeletal muscle and PECAM1(+) ECs followed by vasculatures
43 (Hutcheson and Kardon, 2009; Kardon et al., 2002; Lagha et al., 2009; Mayeuf-Louchart et al.,
44 2014; Mayeuf-Louchart et al., 2016). In addition, FLK1(+) cells give rise to myogenic cells
45 during development and oncologic transformation (Drummond and Hatley, 2018; Mayeuf-
46 Louchart et al., 2014; Motoike et al., 2003). Lastly, multipotent mesoangioblasts, vessel-
47 associated stem cells, have been identified in embryonic dorsal aorta (Minasi et al., 2002). These
48 cells are able to differentiate into several types of mesodermal tissues including skeletal muscle
49 and ECs (Roobrouck et al., 2011). Interestingly, these myogenic cells show the same
50 morphology as muscle satellite cells (MuSCs), stem cell populations for skeletal muscle, and
51 express a number of myogenic and EC markers such as MyoD, M-cadherin, FLK1 and VE-
52 cadherin (De Angelis et al., 1999). However, it is not clear whether adult MuSCs derived from
53 these bipotent progenitors still maintain canonical EC signals. Curiously, blood vessel-associated
54 myoendothelial cell progenitors that express both myogenic and EC markers, and are able to
55 differentiate into myogenic cells following transplantation have been identified in the interstitial
56 spaces of both murine and human adult skeletal muscle (Tamaki et al., 2002; Zheng et al., 2007;
57 Huang et al., 2014). However, the relationship between these myoendothelial cell progenitors
58 and MuSCs remains unclear.

59

60 Vascular endothelial growth factor (VEGF), specifically VEGFA modulates many
61 biological aspects including angiogenesis through its two receptors, FLT1 and FLK1. Although
62 FLK1 possesses stronger signaling capability and the major signaling receptor tyrosine kinase
63 (RTK) for VEGFA, FLT1 has considerably higher affinity for VEGF but weaker cytoplasmic
64 signaling capability. In normal tissue, FLT1 acts as a decoy receptor and a sink trap for VEGF
65 thereby preventing excessive normal and pathological angiogenesis. In addition, there are two
66 co-receptors for VEGFA (NRP1 and NRP2) that function with FLK1 to modulate VEGFA
67 signaling. While VEGF signaling has been extensively studied for its role in development,
68 proliferation, and survival of endothelial cells (ECs), its role in non-vascular systems such as
69 neuron and bone has only recently been appreciated (Liu et al., 2012; Okabe et al., 2014; Poesen
70 et al., 2008). Skeletal muscle tissue is the most abundant producer of VEGFA in the body. It has
71 already been extensively studied in the skeletal muscle fibers in models of *Vegfa* knockout mice
72 (Olfert et al., 2009; Tang et al., 2004; Wagner et al., 2006) as well as *Vegfa* overexpression
73 (Arsic et al., 2004; Bouchentouf et al., 2008; Messina et al., 2007; Yan et al., 2005).

74 Adult skeletal muscle also contains the tissue resident muscle stem cell population,
75 termed MuSCs, which mediate postnatal muscle growth and muscle regeneration (Motohashi and
76 Asakura, 2014). After muscle injury, quiescent MuSCs initiate proliferation to produce myogenic
77 precursor cells, or myoblasts. The myoblasts undergo multiple rounds of cell division before
78 terminal differentiation and formation of multinucleated myotubes by cell fusion. Importantly,
79 the MuSC-derived myoblasts also express VEGFA, which has been shown to increase the
80 proliferation of myoblasts (Christov et al., 2007). Our data obtained from genetical model mice
81 demonstrated that MuSCs express abundant VEGFA, which recruits ECs to establish vascular

82 niche for MuSC self-renewal and maintenance (Verma et al., 2018). In addition, VEGFA and its
83 receptors are expressed in the myoblast cell line, C2C12 cells, and the signaling can induce cell
84 migration and protect apoptotic cell during myogenic differentiation *in vitro* (Bryan et al., 2008;
85 Germani et al., 2003; Mercatelli et al., 2010). However, it is not clear whether MuSCs also
86 express VEGF receptors and if cell-autonomous VEGFA signaling plays an essential roles in
87 MuSC fucction during muscle regeneration *in vivo*.

88 We have previously shown that *Flt1* heterozygous gene knockout and conditional
89 deletion of *Flt1* in ECs display increased capillary density in skeletal muscle, indicating the
90 essential roles for *Flt1* in adult skeletal muscle. More importantly, when crossed with the
91 Duchenne muscular dystrophy (DMD) model *mdx* mice, these mice show both histological and
92 functional improvements of their dystrophic phenotypes. This was due to the effect of increased
93 ECs leading to an increase in MuSCs (Verma et al., 2010; Verma et al., 2019). However, the
94 effect of VEGFA on MuSC *in vivo* remained unknown. We found that MuSCs express low levels
95 of canonical EC markers including VEGF receptors using single cell transcriptomics. Therefore,
96 we examined the effects of VEGFA on MuSCs and show that it has a drastic effect on cell
97 survival in the via its receptor FLT1 by signaling through AKT1.

98

99 **Results**

100 **EC gene signal including *Vegf receptors* in MuSCs**

101 EC signatures in MuSCs has been seen in several gene expression data sets (Figure S1A-D,
102 Table S1) (Fukada et al., 2007; Ryall et al., 2015; van Velthoven et al., 2017; Yue et al., 2020).
103 However, with the lack of EC control, we questioned whether these were true expression or
104 artifact. To isolate EC and MuSC populations, we first crossed the *Flk1*$^{+/GFP}$ mice to label the

105 ECs of the vasculature (Ema et al., 2006) and the *Pax7*$^{+/CreERT2}$:*ROSA26*$^{+/Loxp\text{-}stop\text{-}Loxp\text{-}tdTomato}$
106 (*Pax7*$^{+/CreERT2}$:*R26R*$^{+/tdT}$) mice to mark the MuSC lineage (Murphy et al., 2011; Verma et al.,
107 2018). We performed bulk RNA sequencing (RNAseq) on FACS sorted ECs and MuSCs as well
108 as freshly isolated single muscle fibers (Figure 1A, S1E-G). We found that single muscle fibers
109 routinely have ECs fragments attached to the fiber (Figure S1G) and so we removed such fibers
110 based of Flk1$^{GFP}$ expression from the samples collected for sequencing. We surveyed for
111 canonical genes for each cell type (Figure 1B) and found minimal but reliable expression of
112 canonical ECs genes such as *Pecam1*, *Cdh5*, *Kdr*, and *Flt1* in MuSCs.

113 It is possible that these EC signatures detecting in MuSCs were not due to small amounts
114 of contaminating ECs with very high expression of the canonical EC genes skewing the average
115 expression in MuSC RNA samples. To rule out this possibility, we performed single cell
116 RNAseq (scRNAseq) on MuSCs and ECs isolated from mouse hind limb muscle from both basal
117 condition and 3-days post injury to look at both quiescent and activated MuSCs from the reporter
118 mice specified above (Figure 1A). We could reliably delineate injured and activated MuSCs via
119 side and forward scatter (Figure S1H, S1I). We FACS isolated cells from both days separately
120 and spiked in 20% of the ECs into the MuSCs, and performed scRNAseq for each time point
121 (Figure 1A). We performed sequencing with ~300K read/cell compared with the commonly used
122 sequencing with 60K reads/cell, in order to maximize the possibility of detecting low abundance
123 transcripts (Zhang et al., 2020). In the aggregated dataset, the MuSCs showed low overlap
124 between D0 and D3 owing to the different stages of the myogenic differentiation cycle, while the
125 ECs clusters showed near perfect overlap (Figure 1C, 1D). While drastic morphological changes
126 in ECs have been shown during muscle regeneration (Hardy et al., 2016), transcriptomic changes
127 are much more tapered, especially compared with MuSCs (Latroche et al., 2017). We were able

128 to deconvolve the quiescent MuSCs from the activated and differentiating MuSCs, ECs, and
129 other cell types from gene signatures. (Figure S1J). We also introduced an artificial chromosome
130 loci in our sequencing reference genome to allow for mapping of custom genes such as *eGFP-*
131 *SV40* and *tdTomato-WPRE-BGHPolyA* transgenes and were able to confirm high expression of
132 these genes to their respective clusters (Figure 1E). Importantly, data from scRNAseq were able
133 to recapitulate the minimal expression of canonical EC genes in the MuSC clusters such as *Cdh5*
134 (Figure 1E) as seen in our Bulk RNAseq results (Figure 1B). These included the *Vegf receptors*
135 *Flk1* (*Kdr*) and *Flt1* (Figure 1E).

136 As a quality control measure, we mapped parts of the three transgene genes, *eGFP* from
137 *Flk1*$^{+/GFP}$, and *tdTomato* and *CreERT2* from *Pax7*$^{+/CreERT2}$*:R26R*$^{+/tdT}$ that can be detected in ECs
138 and MuSCs, respectively, as expected (Figure S1L). Surprisingly, we also found *eGFP* in the
139 MuSCs and *tdTomato* in EC fraction, while the *CreERT2* expression remained mainly restricted
140 to the MuSCs (Figure S1K). FACS analysis and FACS-sorted cells confirmed that GFP(+) and
141 tdTomato(+) cells are exclusively restricted as ECs and MuSCs, respectively (Figure S1E, S1F).
142 Therefore, we hypothesized that this was due to the ambient free mRNA from the digested cells
143 that is intrinsic to any droplet based single cell sequencing platform. By using SoupX (Young
144 and Behjati, 2020), we performed careful background subtraction using genes expressed
145 exclusively in myofibers as our negative control and genes validated by *in situ* hybridization as a
146 positive control (Figure S1K) (Kann and Krauss, 2019). We observed decreased but sustained
147 *eGFP* expression in the MuSC fraction and *tdTomato* expression in the EC fraction after SoupX
148 subtraction (Figure S1K). In addition, the EC signatures such as *Cdh5* expression in the MuSC
149 fraction was also sustained. These results conclude that MuSCs contain mRNAs from canonical

150 ECs genes. We showed that the canonical EC genes were broadly expressed in the myogenic
151 cells in our dataset (Figure 1E).

152 Since detection of rare subpopulation in single cell dataset is a factor of cell numbers, we
153 re-analyzed previously published dataset with 2,232 myogenic cells across different states (Torre
154 et al., 2018; De Micheli et al., 2020). We were able to classify cell as quiescent, proliferative vs.
155 differentiating states based on the expression of *Calcr*, *Cdk1* and *Myog*, respectively (Figure
156 S1L). We noticed that EC prototypic markers such as *Flt1* are broadly expressed with small
157 amounts in MuSCs. Complementary data from different laboratories showed the clear expression
158 of EC prototypic markers such as *Cdh5*, *Flt1* and *Kdr*, using microarrays and Bulk-RNAseq
159 (Figure S1A, S1B; Fukada et al., 2007; Ryall et al., 2015). Recently, RNAseq data from fixed
160 quiescent, early activated and late activated MuSCs show that *Flt1* may be transiently
161 upregulated during the early activation process (Figure S1C) (Yue et al., 2020). To confirm
162 whether the EC gene mRNAs were transcribed from MuSCs, we utilized previously published
163 MuSC nascent RNA transcriptome from TU-tagged samples (Gay et al., 2013; van Velthoven et
164 al., 2017). As expected, *Myh1* was represented in the whole muscle but was absent in the TU-
165 tagged MuSCs (Figure 1F), indicating that the nascent MuSCs were devoid of cellular
166 contamination from other cells in the muscle. Inversely, the nascent MuSC transcript was over-
167 represented for MuSC related genes such as *Calcr* and *Sdc4*. Interestingly, we were able to detect
168 EC genes such as *Kdr* and *Pecam1* in the TU-tagged MuSC samples indicating that they were
169 actively transcribed by MuSCs (Figures 1F, S1D).

170 We also verified the expression of *Vegfr* genes (*Kdr*, *Flt1*, *Nrp1* and *Nrp2*) in MuSCs
171 using RT-qPCR (Figure 1G). In addition, we verified the expression of *Flt1* by performing *in-*
172 *situ* hybridization using RNAScope on MuSC on whole muscle fiber, which we currently believe

173 to be the gold standard for expression studies (Figure 1H). Finally, in MuSC-derived myoblasts,
174 NRP1and NRP2 expression was detectable with comparable intensity compared with EC cell
175 line, while FLT1 expression was detectable with lower intensity compared with EC cell line
176 (Figure 1I). By contrast, PECAM1, VE-Cadherin and FLK1 expression, which was clearly
177 detected in EC cell line, was undetectable level in myoblasts. Taken together, these data indicate
178 that there are both transcripts of these EC canonical genes and EC canonical proteins in MuSCs.
179

180 **VEGFA induces proliferation and cell survival but not differentiation in myoblasts**

181 Since VEGFRs were expressed in MuSCs in small amounts and their ligand, VEGFA, was
182 highly expressed in MuSCs (Figure 2A; Verma et al., 2018), we wanted to investigate whether
183 there were any biological effects to induction by VEGFA. We found that treatment with VEGFA
184 could increase proliferation of MuSC-derived myoblasts at low dose but inhibit proliferation at
185 high dose of VEGFA, a phenomenon that has been previously described in ECs (Noren et al.,
186 2016) (Figure S2A). We saw no effect on differentiation by VEGFA as evaluated by myosin
187 heavy chain (MyHC) staining, fusion index and RT-qPCR (Figure S2B, S2C, S2D). By contrast,
188 crystal violet staining showed that VEGFA could significantly increase survived cell number of
189 myoblasts following UV-mediated apoptotic cell death induction (Figure S2E, S2F). To
190 investigate apoptosis in detail, we optimized Annexin V assay following thapsigargin-mediated
191 endoplasmic reticulum (ER)-stress (Hirai et al., 2010) so that we could study deviation at ~ED50
192 while still performing experiments to remove the confounding variable to proliferation from the
193 experimental setup (Figure S2G and S2H). We had previously shown that MuSCs are the
194 predominant cells that secrete VEGFA in skeletal muscle (Figure 2A; Verma et al., 2018) and
195 while adding exogenous VEGFA did not improve cell survival, blocking VEGFA via a soluble

196 form of FLT1-FC increased the number of apoptotic and necrotic myoblasts *in vitro* (Figure 2C-
197 E).
198
199 **VEGFA-facilitated cell survival in MuSC-derived myoblasts is mediated through FLT1**
200 To characterize the VEGF receptor responsible for the anti-apoptotic effect of VEGFA on
201 MuSC-derived myoblasts, we used pharmacological inhibitors of the VEGF receptors (Figure
202 2F). We used blocking antibody for the VEGF receptors FLT1 (anti-FLT1 antibody), small
203 molecule inhibitors for FLK1 (SU4502 and ZM306416) and the FLK1 co-receptor NRP1
204 (EG00229) following thapsigargin induction (Figure 2D). Surprisingly, inhibiting FLK1, the
205 major signaling RTK for VEGFA, had no effect on myoblasts survival following thapsigargin
206 induction (Figure 3E). By contrast, blocking FLT1 via blocking antibody greatly decreased the
207 survival of myoblasts following thapsigargin induction (Figure 3E). To confirm this interesting
208 result using genetic tools, we obtained myoblasts with *Pax7-CreER*-inducible deletion of *Flt1*
209 mice ($Pax7^{+/CreER}$:$Flt1^{Loxp/Loxp}$ or *MuSC-*$Flt1^{\Delta/\Delta}$) and the control mice ($Pax7^{+/+}$:$Flt1^{Loxp/Loxp}$). *In*
210 *vitro* 4-OHT-mediated genetic deletion of *Flt1* (MuSC-$Flt1^{\Delta/\Delta}$) resulted in down-regulation of
211 *Flt1* RNA and FLT1 protein expression (Figure S2I, S2J), and increased spontaneous apoptotic
212 cell death even without induction of apoptosis (Figure 2F). By contrast, *Flt1* deletion did not
213 affect cell proliferation assessed by EdU staining or myogenic differentiation assessed by MyHC
214 staining (Figure S2K-M). When thapsigargin-induced apoptosis was induced, the *MuSC-*$Flt1^{\Delta/\Delta}$
215 myoblasts had increased apoptosis that was not responsive to exogenous VEGFA (Figure 2G).
216
217 **AKT signaling is involved in apoptosis of muscle stem cells.**

218 VEGFA signaling is mediated through Extracellular signal-Regulated Kinase (ERK), p38
219 Mitogen-Activated Protein Kinase (MAPK), and Protein kinase B (AKT). In ECs, VEGFA is
220 known to protect cells from apoptosis via AKT (Domigan et al., 2015; Lee et al., 2007).
221 However, it is not known whether VEGFA can similarly activate AKT in MuSC-derived
222 myoblasts. While the role of AKT has been explored in proliferation and differentiation in
223 myoblasts, its role in apoptosis has not been well characterized (Loiben et al., 2017). We
224 assessed for AKT activation via phosphorylated AKT (pAKT) in MuSC-derived myoblasts. We
225 found that exogenous VEGFA could induce AKT phosphorylation (pAKT) (Figure 2H, 2I). This
226 response was blunted in *MuSC-Flt1*$^{\Delta/\Delta}$ myoblasts and was no longer responsive to VEGFA
227 (Figure 2H, 2I). Lastly, we wanted to confirm that AKT activation could improve myoblast
228 survival. We infected lentiviral *E4ORF1* or *MyrAKT* vectors in myoblasts (Figure 2J), both of
229 which gene products have been shown to specifically activate AKT without activating ERK or
230 p38 (Kobayashi et al., 2010). We found that overexpression of either of these genes improved
231 cell survival compared with the control *in vitro* following induction of apoptosis via thapsigargin
232 (Figure 2J). These data establish FLT1-AKT as the cascade linking VEGFA to apoptosis in
233 MuSC-derived myoblasts during muscle regeneration (Figure 2K).
234

235 **VEGFA-FLT1 pathway protects MuSCs from apoptosis *in vivo***

236 Endogenous and exogenous VEGFA have been shown to regulate cell survival and protect ECs
237 from apoptosis *in vitro* (Gerber et al., 1998; Lee et al., 2007). To assess whether additional
238 VEGFA had an effect of MuSC behaviors *in vivo*, we used mice carrying the *VEGFA*$^{+/Hyper}$ allele
239 for injury-mediated tibialis anterior (TA) muscle regeneration following $BaCl_2$ injection (Figure
240 3A, 3B) (Miquerol et al., 1999). MuSC-derived myoblasts from *Pax7*$^{+/tdT}$*:VEGFA*$^{+/Hyper}$ mice

241 showed around 2.8 fold increased expression of *Vegfa* but not the *Vegfrs* compared with
242 myoblasts from wild-type mice (Figure S3A). Interestingly, while treatment with VEGFA alone
243 had no effect on apoptosis *in vitro*, the MuSCs from *Pax7*$^{+/tdT}$*:VEGFA*$^{+/Hyper}$ mice showed
244 decreased cell death in regenerating muscle by 1 day following $BaCl_2$ injection (Figure 3C).
245 Consequently, single muscle fibers from *Pax7*$^{+/tdT}$*:VEGFA*$^{+/Hyper}$ mice showed increased number
246 of MuSCs, compared with those from *Pax7*$^{+/tdT}$*:VEGFA*$^{+/+}$ mice by 28 days following $BaCl_2$
247 injection (Figure 3D). In addition, muscle regeneration was promoted in *VEGFA*$^{+/Hyper}$ mice in
248 the early and late muscle repair processes as judged by fiber diameter (Figures 3B, 3E, 3F, S3B-
249 D).

250 We then performed the reciprocal experiment to investigate the consequence of *Vegfa*
251 loss in MuSCs *in vivo*, and utilized MuSC-specific *Vegfa* knockout mice
252 (*Pax7*$^{+/CreER}$*:VEGFA*$^{Loxp/Loxp}$). We have previously shown that vasculature in the MuSC-
253 *VEGFA*$^{\Delta/\Delta}$ mouse muscle is perturbed and the proximity between the MuSC and EC is increased
254 (Verma et al., 2018). However, the functional consequences of this remained unknown. We
255 confirmed that clear downregulatin of VEGFA protein in MuSC-derived myoblasts isolated from
256 MuSC-*VEGFA*$^{\Delta/\Delta}$ mice (Figure S3E). We noticed that deletion of *Vegfa* in MuSCs in the *MuSC-*
257 *VEGFA*$^{\Delta/\Delta}$ mouse muscle led to an increase in the proportion of dead MuSCs following $BaCl_2$
258 injection (Figure 3G). Consequently, the number of MuSCs in the MuSC-*VEGFA*$^{\Delta/\Delta}$ muscle were
259 significantly reduced following recovery after injury (Figure 3H). There was no difference in the
260 MuSC numbers in MuSC-*VEGFA*$^{\Delta/\Delta}$ muscle at homeostasis. In addition, the muscle had a
261 regenerative defect as indicated by the shift in fiber size distribution and increased adipose
262 following muscle injury (Figure 3B, 3I, 3J, S3F-H). While a limitation of this experiment is that
263 the MuSC fusion into the fiber also deletes *Vegfa* from the fiber themselves, muscle fiber

264 specific deletion of *Vegfa* has not shown to have an effect on fiber size (Delavar et al., 2014).
265 These data indicate that cell intrinsic VEGFA improves cell survival of MuSCs and that loss of
266 MuSC-derived VEGFA results in reduced muscle regeneration.

267 Since FLT1 but not FLK1 was detected in MuSCs and MuSC-derived myoblasts, we
268 asked whether the *Flt1* had an effect on MuSC survival *in vivo,* we evaluated cell death in
269 MuSCs from *MuSC-Flt1*$^{\Delta/\Delta}$ mouse muscle. We induced muscle regeneration using $BaCl_2$ for 1
270 day and assessed for cell death in MuSCs. As seen *in vitro*, we found that loss of *Flt1* in MuSCs
271 (Figure S2I, S2J) resulted in increased cell death during early regeneration (Figure 3K).
272 Consequently, single muscle fibers from *MuSC-Flt1*$^{\Delta/\Delta}$ mice showed decreased number of
273 MuSCs, compared with those from *MuSC-Flt1*$^{+/+}$ mice by 28 days following $BaCl_2$ injection
274 (Figure 3L). We also examined the long-term *in vivo* consequence of deleting *Flt1* from MuSC.
275 There was no significant muscle phenotype in MuSC-*Flt1*$^{\Delta/\Delta}$ muscle at homeostasis (Figures 3B,
276 3M, 3N). However, following injury, the MuSC-*Flt1*$^{\Delta/\Delta}$ muscle had a modest regenerative defect
277 as indicated by the shift in fiber size distribution following muscle injury (Figures 3B, 3M, 3N,
278 S3J-N).

279

280 **VEGFA-FLT1 pathway regulates muscle pathology in DMD model mice**

281 While angiogenic defects have been reported in the *mdx* mice as well as in golden retrieval
282 muscular dystrophy (GRMD; canine model of DMD) (Latroche et al., 2015; Verma et al., 2019,
283 2010; Kodippili et al., 2021; Podkalicka et al., 2021), it is not clear whether VEGF family and its
284 receptors are implicated in human dystrophinopathies. We probed the VEGF ligands and
285 receptors in microarrays (Table S1) from skeletal muscles and MuSCs from *mdx* mice
286 (Pallafacchina et al., 2010; Tseng et al., 2002) and skeletal muscles from the *GRMD* (Vieira et al.,

287 2015). *Vegfa* was downregulated in both models (Figure S4A). *Flt1* was also downregulated in
288 *GRMD* but not *mdx* muscles. To examine whether VEGF signaling is altered in DMD patients,
289 we performed gene expression analysis on previously available data from microarrays from
290 patients with DMD (Chen et al., 2000). We also aggregated and probed microarray data from
291 muscle biopsies of patients with various neuromuscular diseases or of healthy individuals after
292 exercise (Bakay et al., 2006). In the microarray data, *Vegfa* expression was increased after an
293 acute bout of exercise, and *Vegfa* expression was reduced in ALS muscle, BMD muscle, as well
294 as both early and late phases of DMD muscle (Figure S4A). These data indicate that *Vegfa*
295 expression is decreased in dystrophinopathy, and thus may benefit people with DMD by
296 increasing VEGFA as a therapeutic target.

297 Therefore, we crossed the *MuSC-Flt1*$^{\Delta/\Delta}$ mice with the chronically regenerating DMD
298 model mice (*mdx*) to generate *mdx:MuSC-Flt1*$^{\Delta/\Delta}$ mice, and analyzed long term effects of *Flt1*
299 deletion (Figure 4A, S4B). Importantly, we found a significant decrease in fiber diameter and
300 increased fibrosis (Figures 4B-D, S4C) in TA muscle accompanied by a physiological decease in
301 muscle perfusion as shown by laser Doppler flow at 12 months age (Figure 4E) as well as a
302 functional decline in muscle strength as judged by grip strength both acutely and chronically
303 (Figure 4F).

304 By contrast, when we crossed the *VEGFA*$^{+/Hyper}$ mice with *mdx* mice (Figure 4A, S4D),
305 we noticed a significant increase in fiber diameter and decreased fibrosis (Figures 4G-J, S4E) in
306 both TA and diaphragm muscle of *mdx:VEGFA*$^{+/Hyper}$ mice accompanied by a physiological
307 increase in muscle perfusion as shown by laser Doppler flow at 12 months age (Figure 4K) as
308 well as a functional increase in muscle strength as judged by grip strength (Figure 4L). These

309 data indicate that VEGFA-FLT1 axis is a therapeutic target for the pathology seen in the *mdx*
310 mice
311
312 **Discussion**
313 In this report, we performed bulk and single cell RNA sequencing on MuSCs and ECs. Since
314 deep reads can significantly reduce the effect of the technical noise in scRNAseq, it can improve
315 estimation of minor transcriptional state of a given cell (Zhang, 2020). Unexpectedly, we found
316 that MuSCs broadly express EC prototypic markers in small amounts and used multiple different
317 bioinformatics techniques to validate the results. While similar phenomenon in myogenic cells
318 during development and existence of blood vessel-associated myoendothelial cells in the adult
319 skeletal muscle have been previously described, no functional follow up as been performed
320 leading to the questions whether these minor expression profiles were artifacts or functional (De
321 Angelis et al., 1999; Minasi, 2002; Tamaki et al., 2002; Zheng et al., 2007; Roobrouck, 2011;
322 Huang et al., 2014; Charville et al., 2015; Goel et al., 2017; Giordani et al., 2018). Our goal was
323 to see whether this small expression pattern had biological consequences. We ultimately decided
324 to use *Flt1* for further investigations and used RNAscope and immunostaining to validate its
325 expression in MuSCs. We found that *Flt1* indeed exerts a biological function even at a low
326 expression. Signaling through VEGFA-FLT1-AKT can improve cell survival in MuSCs both *in*
327 *vivo* and *in vitro.*
328 On a grander scale, our finding of EC prototype markers expressed in MuSC calls into
329 two questions 1) the genes that we used to specify cellular identities and 2) the cellular identity
330 of MuSCs and ECs. The former is important as when we experimentally label, induce or perform
331 Cre-mediated gene knockout experiments based on our assumptions of different gene expression

332 results which may be confounded for these low expressing genes. For example, we have
333 previously investigated both *Flt1* and *Kdr* in mouse muscle using three different reporters and
334 found them to be negative in MuSCs, thereby disregarding their cell-autonomous effect when
335 evaluating global knockouts (Verma et al., 2018, 2010). It is also possible that EC mRNAs are
336 results of transcription from the cell or a result of mRNA transfer from neighboring cells
337 (Desrochers et al., 2016). Of note, the transmission of *tdTomato* mRNA and protein from
338 $Pax7^{+/CreERT2}$:$R26R^{+/tdT}$ mice used in this study has been recently shown via exosome, opening
339 up the possibility of transmission of other mRNA from MuSC to ECs (Murach et al., 2020). The
340 later is an interesting phenomenon form a developmental point of view. MuSCs and ECs arise
341 from a bipotent progenitor originated from somites during early development (Kardon et al.,
342 2002; Hutcheson, 2009; Lagha, 2009; Mayeuf-Louchart, 2014; Mayeuf-Louchart, 2016).
343 Therefore, it is possible that there is a permissive chromatin state that allows for expression of
344 reciprocal genes in the two populations. Along the lines of these observations, FLK1(+) or VE-
345 cadherin(+) cells can contribute to myogenic cells *in vitro* and after cell transplantation (Tamaki
346 et al., 2002; Le Grand et al., 2004; Zheng et al., 2007; Huang et al., 2014;), and during
347 development (Drummond and Hatley, 2018; Mayeuf-Louchart et al., 2014; Motoike et al., 2003).
348 Important notion is that the PDGFRα(-)FLK1(+) population exhibited restricted potential to
349 differentiate into the MuSCs in injured muscle (Sakurai et al., 2008). Interestingly, in the
350 zebrafish, exogenous expression of *Etv2* in the fast muscle can lead to transdifferentiation of
351 muscle fibers into functional vessels so there is evidence of cell fate flexibility (Veldman et al.,
352 2013). The potential of EC transdifferentiation was also examined by ETV2 overexpression in
353 five human cell types, skeletal muscle cells, adipose-derived mesenchymal stem cells, umbilical
354 cord-derived mesenchymal stem cells, embryonic lung fibroblast cells and skin fibroblast cells.

355 Among them, human skeletal muscle cells showed the highest amenability for this EC induction
356 following infection with ETV2 lentivirus vector (Yan et al., 2019). Conversely, *Etv2*-deficient
357 vascular progenitors can differentiate into skeletal muscle cells (Chestnut et al., 2020). It would
358 be interesting to see whether other EC gene signatures also have functional consequences in the
359 MuSC or muscle at large.

360 We decided to focus on function of *Flt1* among several EC genes expressed in MuSCs
361 for further investigations on MuSC biology. Our pharmacological and genetic analyses
362 demonstrate that MuSC-derived VEGFA has a drastic effect on cell survival in the via its
363 receptor FLT1 by signaling through AKT1. While VEGFA binds to both FLT1 and FLK1,
364 VEGFB and PGF only bind to FLT1. This creates a scenario where PGF and VEGFB binding
365 can sequester FLT1, increasing free VEGFA availability for VEGFA-FLK1 binding which is the
366 major VEGF signaling pathway for many cell types (Vempati et al., 2014). While PGF is not
367 normally expressed in adult tissues, VEGFB is expressed in the MuSCs and muscle fiber (data
368 not shown). Importantly, the VEGFB-FLT1 axis has also been shown to inhibit apoptosis in
369 retina and brain cells in mouse models of ocular neurodegeneration and stroke (Li et al., 2008).
370 While our results cannot rule out the involvement of VEGFB in protection of MuSC apoptosis,
371 we provide evidence from both pharmacological and genetic data to indicate that VEGFA is
372 involved.

373 Despite drastic effect of VEGFA-FLT1 on apoptosis *in vitro*, the long-term consequences
374 of *in vivo* deletion of *Flt1* in the MuSC compartment were modest compared with deletion of
375 *Vegfa* in the MuSCs unless crossing with *mdx* mice. Although *Vegfa* is required for both MuSC
376 survival and recruitment of vascular niche (Verma et al., 2018), in the steady state, the MuSC
377 turnover may be low enough that the apoptotic stress burden is low. VEGFA improves cell

378 survival during the proliferative stage following injury, however this transient improvement in
379 survival has only a modest impact on the final regenerative process as shown in
380 *mdx:VEGFA*$^{+/Hyper}$ mice.

381 VEGFA and FLT1 targeted therapies are being explored as both pro- and anti-angiogenic
382 therapies for several indications including retinal degeneration, cancer, pre-eclampsia and
383 neuromuscular diseases (Bae et al., 2005; Keifer et al., 2014; Mac Gabhann et al., 2011; Verma
384 et al., 2010; Verma et al., 2019; Bosco et al., 2021; Xin et al., 2021). As these therapies mature,
385 it will be important to ascertain the MuSC-specific effects of VEGFA and FLT1.

386

387 **Materials and Methods**

388 **Mice**

389 *Flt1*$^{LoxP/LoxP}$ were obtained from Gua-Hua Fong (Ho et al., 2012). *B6.Cg-Pax7*$^{tm1(cre/ERT2)Gaka/J}$
390 (*Pax7*$^{+/CreERT2}$; JAX stock# 017763; Murphy et al., 2011), *B6.Cg-Gt(ROSA)*$^{26Sortm9(CAG-tdTomato)Hze/J}$
391 (*Ai9*; JAX stock # 007909; Madisen et al., 2010), *VEGFA*$^{+/Hyper}$ (*Vegfatm1.1Nagy/J*; JAX stock#
392 027314; Miquerol et al., 1999) and *B6Ros.Cg-Dmd*$^{mdx-5cv}$*/J* (*mdx*$^{5cv}$; JAX stock #002379;
393 Chapman et al., 1989) were obtained from Jackson Laboratory. *Kdr*$^{tm2.1Jrt/J}$ (*Flk1*$^{+/GFP}$) were
394 obtained from Masatsugu Ema (Ema et al., 2006). *B6.Cg-Pax7*$^{tm1(cre/ERT2)Gaka/J}$ (*Pax7*$^{+/CreERT2}$)
395 mice were crossed with the *B6.Cg-Gt(ROSA)*$^{26Sortm9(CAG-tdTomato)Hze/J}$ (*Ai9*) to yield the
396 *Pax7*$^{+/CreERT2}$*:R26R*$^{tdT}$(*Pax7*$^{tdT}$) mice. *Pax7*$^{tdT}$ mice were bred with the *VEGFA*$^{+/Hyper}$ and
397 *Flk1*$^{+/GFP}$ to obtain *Pax7*$^{+/tdT}$:*VEGFA*$^{+/Hyper}$ and *Pax7*$^{+/tdT}$*:Flk1*$^{+/GFP}$ mice. *VEGFA*$^{LoxP/LoxP}$ mice
398 obtained from Napoleone Ferrara (Gerber et al., 1999) were crossed with *Pax7*$^{+/CreERT2}$ to yield
399 the *Pax7*$^{+/CreERT}$*: VEGFA*$^{LoxP/LoxP}$ mice. *Flt1*$^{LoxP/LoxP}$ mice obtained from Guo-Hua Fong (Ho et al.,
400 2012) were crossed with *Pax7*$^{+/CreERT2}$ to yield the *Pax7*$^{+/CreERT}$*:Flt1*$^{LoxP/LoxP}$ mice. Colonies for all
401 the mice were established in the laboratory. Cre recombination was induced using tamoxifen
402 (Sigma-Aldrich, T5648) dosed as 75 mg/kg body weight x 3 times over one week at 3-6 weeks
403 of age. Mice carrying the wild-type *CreERT2* allele were used for control experiments. TA
404 muscle regeneration was induced by intramuscular injection of 20 µl of 1% $BaCl_2$ (Sigma-
405 Aldrich, 342920) or 20 µl of 10 µM Cardiotoxin (CTX) (Sigma-Aldrich, V9125). Mice used for
406 this study is summeried in Table S2.

407 Genotyping to detect the transgenic and mutant alleles was performed by PCR using the
408 primers described on the web site of Jackson Laboratory shown in Table S3. All primers were
409 synthesized as custom DNA oligos from Integrated DNA technologies (IDT). Genotyping to

410 detect the mutated allele of *mdx*$^{5cv}$ was performed by PCR using the primers (0981 and 0982)
411 shown in Table S1. The PCR product DNA was digested with *Dra*III restriction enzyme (New
412 England Biolabs, R3510S). Wild-type allele generated 180 bp and mutant allele generated 50
413 and 130 bp bands.

414 The animals were housed in an SPF environment and were monitored by the Research
415 Animal Resources (RAR) of the University of Minnesota. All protocols were approved by the
416 Institutional Animal Care and Usage Committee (IACUC) of the University of Minnesota and
417 complied with the NIH guidelines for the use of animals in research.

418

419 **Cell isolation by FACS**

420 *Pax7*$^{tdT}$*:Flk1*$^{GFP}$ mice were utilized for FACS-mediated MuSC and EC isolation as previously
421 described (Asakura et al, 2002; Verma, 2018). We performed extensive validation of the
422 fluorescent reporter mice as previously described (Figure S1A-C; Verma, 2018). Briefly,
423 quiescnet MuSCs and ECs were isolated from the hind limb skeletal muscle of 1–2-mo-old
424 *Pax7*$^{tdT}$*:Flk1*$^{GFP}$ mice after digestion with collagenase type II. FACS was performed on an FACS
425 sorter (BD FACSAria) and data were analyzed using FlowJo (BD Biosciences). Sorting gates,
426 tdTomato(+) for MuSCs and GFP(+) for ECs, were strictly defined based on control cells
427 isolated from wild-type mice and the forward scatter and side scatter gating. Sorted cells were
428 immediately characterized by immunostaining on slide glasses, utilzed for RNA preparation or
429 cultured on collagen-coated plates in the myoblast growth medium as below to obtain MuSC-
430 derived myoblasts and ECs. FACS analysis was performed as previously described (Turaç et al.,
431 2013). Cells were either trypsinized (cultured cells) or a single cell suspension was obtained
432 following enzymatic digestion as whole muscle-derived cells (Asakura, 2002). Cells were then

433 washed with FACS buffer (2% BSA and 1 mM EDTA in PBS) followed by live/dead staining
434 using ZombieNIR (Biolegends, 423105). Cells were washed, then immunostained for cell
435 surface markers. Blocking cells was performed with 1% BSA/PBS, and cells were incubated in
436 fluorescently-conjugated antibody. FACS was performed on a Fortessa X-20 (BD Biosciences)
437 with a 355 nm, 405 nm, 488 nm, 561 nm, and 640 nm lasers.
438
439 **Cell culture**
440 MuSC-derived myoblast isolation from adult mice was performed as previously described
441 (Asakura et al, 2001; Motohashi et al., 2014). Briefly, after collagenase type II (Worthington,
442 CLS-2) treatment, dissociated cells from mouse hindlimb muscle were incubated with anti-
443 CD31-PE (eBiosciences, 12-0311), anti-CD45-PE (eBiosciences, 30-F11), anti-Sca1-PE
444 (eBiosciences, Dec-81) and anti-Integrin α7 (MBL International, ABIN487462), followed by
445 anti-PE microbeads (Miltenyi Biotec, 130-048-801), and then performed LD column (Miltenyi
446 Biotec, 130-042-901) separation. Negative cell populations will be incubated with anti-Mouse
447 IgG beads (Miltenyi Biotec, 130-048-402), and then MS coulumn (Miltenyi Biotec, 130-042-
448 201) separation was performed to isolate Integrin α7(+) MuSCs. MuSC-derived myoblasts were
449 maintained in culture on collagen coated plates in myoblast medium containing 20% FBS and 20
450 ng/ml bFGF (Invitrogen, PHG0263) in HAM's-F10 medium. Cell cultures were maintained in a
451 humidified incubator at 37°C with 5% $CO_2$ and 5% $O_2$. 4-hydroxy tamoxifen (4-OHT, Sigma-
452 Aldrich, H6278) treatment (1 μM in EtOH) was used to induce *Flt1* deletion in myoblasts
453 isolated from $Flt1^{LoxP/LoxP}$:$Pax7^{CreERT2}$ mice. For cell survival assay, 1 x $10^5$ cells were allowed to
454 adhere for one day and starved overnight in 0.1% FBS in HAM's F10 medium. Then, cells were
455 exposed to 1 μM EdU along with or withpout 2-100 ng/ml recombinant VEGFA (R&D Systems,

456 493-MV) for 8 hours before being fixed and stained by the Click-iT EdU Alexa Fluor 488
457 Imaging Kit (Thermo Scientific, C10337). For induction of apoptosis in myoblasts, (1-2 x $10^5$)
458 cells were allowed to adhere to the plates for 16 hours. Thapsigargin-mediated apoptosis was
459 induced by 1 μM of thapsigargin (Sigma-Aldrich, T9033) dissolved in EtOH with or without
460 VEGFA, 100 ng/ml recombinant FLT1-FC (R&D Systems, 7756-FL), 1 μg/ml anti-FLT1
461 monoclonal antibody (Angio-Proteomie, MAB7072), inhibitors of FLK1, 3 μM ZM306416
462 (R&D Systems, 2499/1) and 10 μM of SU5402 (R&D Systems, 3300/1) and an inhibitor of
463 NRP1, 30 μM of EG00229 (R&D Systems, 6986/10) for 24 hours. UV light-mediated apoptosis
464 was induced by exposing the cells to UV light in cell culture hood for 45 seconds without
465 medium. After UV exposure, cell survival was assessed 24 hours following culture in 0.1% FBS
466 in HAM's F10 medium with or without VEGFA using the Crystal violet Assay Kit (Abcam,
467 ab232855) and quantated the Crystal violet dye after solubilization by absorbance at 570 nm. To
468 induce differentiation of myoblasts, the myoblast medium was replaced with differentiation
469 medium that contained DMEM supplemented with 5% horse serum with or withour VEGFA or
470 bFGF for 1 or 3 days followed by anti-sarcomeric myosin heavy chain antibody (Developmental
471 Study Hybridoma Bank, MF-20).
472
473 **AKT induction**
474 The lentiviral pCCL-E4ORF1 and pCCL-myrAkt1 constructs were a kind gift from Dr. Jason
475 Butler (Kobayashi et al., 2010). 293FT cells (Thermo Fisher Scientific, R70007) were seeded in
476 DMEM with 10% FBS and transfected with the lentivirus vectors along with pCMV-VSV-G
477 (Addgene, 8454), pRSV-Rev (Addgene, 12253), and pMDLg/pRRE (Addgene, 12251) using
478 PolyJet transfection reagent (Signagen Laboratories, SL100688). The culture supernatant of the

479 transfected 293FT cells was added to MuSC-derived myoblast culture with 0.8 μg/ml polybrene
480 (MilliporeSigma, H9268). pAKT1(+) cells were stainined with anti-pAKT antibody (Cell
481 Signaling, 4060).
482
483 **Apoptosis assay**
484 Apoptosis was measured using measured using Annexin V-Biotin Apoptosis Detection Kit
485 (eBioscience™, BMS500BT-100) as per the manufacture's instruction. Streptavidin-conjugated
486 AlexaFluro-488 was used for detection. Propidium Iodide (PI) was used in all assays except
487 when Pax7tdT(+) cells were utilized or when ZombieNIR (Biolegends, 423105) was used. FACS
488 was performed on a Fortessa X-20 (BD Biosciences) equipped with a 355 nm, 405 nm, 488 nm,
489 561 nm, and 640 nm lasers.
490
491 **Immunostaining of cells**
492 Immunostaining for PECAM1, VE-Cadherin, VEGFA, VEGFRs was performed on collagen
493 coated coverslips. Other immunostaining was performed on 30 mm tissue culture plates. Cells
494 were fixed with 2% PFA for 5 minutes and immunostained as previously described (Verma et al.,
495 2010). For membrane receptor staining, cells were permeabilized with 0.01% saponin
496 (ThermoFisher Scientific, ICN10285525) which was kept in the staining solution until the
497 primary antibodies were washed off. At which time, 0.01% Triton-X was added to all the buffers.
498 The antibodies used for this study are listed in Table S4.
499
500 **Single muscle fiber isolation and staining**

501 Extensor digitorum longus (EDL) muscle was dissected and digested with 0.2% collagenase type
502 I (Sigma-Aldrich, C0130) for single muscle fiber isolation as previously described (Verma et al.,
503 2010). Single muscle fibers were fixed with 2% PFA/PBS, permeabilized with 0.2% Triton-
504 X100 and counterstained with DAPI. Anti-Pax7 antibody(+) or tdTomato(+) MuSCs per single
505 muscle fiber were counted manually.
506
507 **RNAscope**
508 RNAscope for *Flt1* transcripts was performed as previously described (Kann and Krauss, 2019)
509 on single muscle fibers from $Pax7^{tdT}$ mice using the RNAscope Probe - Mm-Flt1 (C1) (ACDBio,
510 415541). Briefly, isolated EDL fibers are fixed in 4% PFA, washed with PBS, and dehydrated in
511 100% methanol. Subsequently, fibers are rehydrated in a stepwise gradient of decreasing
512 methanol concentrations in PBS/0.1% Tween-20. Fibers are treated with a proteinase for 10
513 minutes, followed by hybridization, amplification, and fluorophore conjugation steps.
514
515 **Histology**
516 The mouse tibialis anterior (TA) muscle was used for all histological analysis. Tissues were
517 frozen fresh using $LiN_2$ chilled isopentane and stored at -80ºC. Eight µm thick transverse
518 cryosections were used for all histological analysis. Hematoxylin & Eosin (HE) staining were
519 performed as previously described (Verma et al., 2010). Sirius red (Direct Red 80, Sigma-
520 Aldrich, 365548) staining was performed for muscle sections for fibrosis as previously described
521 (Shimizu-Motohashi et al., 2015). Muscle sections were stained in Oil Red O solution (Sigma-
522 Aldrich, O1391-250ML) as previously described (Wang et al., 2017). Microscopic images were
523 captured by a DP-1 digital camera attached to BX51 fluorescence microscope with 10x or 40×

524 UPlanFLN objectives with cellSens Entry 1.11 (all from Olympus). Photoshop (Adobe) and Fiji
525 (NIH) were used for image processing and manually enumerating the fiber diameter (Schindelin
526 et al., 2012).
527
528 **Grip strength test**
529 Forelimb grip strength test was performed following a previously published procedure (Aartsma-
530 Rus and van Putten, 2014). Briefly, mice were gently pulled by the tail after fore limb-grasping a
531 metal bar attached to a force transducer (Grip Strength Meter, Columbus Instruments, 1027CSM-
532 D52). Grip strength tests were performed by the same blinded examiner. Five consecutive grip
533 strength tests were recorded, and then mice were returned to the cage for a resting period of 20
534 minutes. Then, three series of pulls were performed each followed by 20 min resting period. The
535 average of the three highest values out of the 15 values collected was normalized to the body
536 weight for comparison.
537
538 **Muscle perfusion**
539 RBC flux was evaluated using the moorLabTM laser Doppler flow meter as previously described
540 (Verma, 2010) with the MP7a probe that allows for collecting light from a deeper tissue level
541 than standard probes according to the manufacturer's instructions (Moor Instruments). The fur
542 from the right hind leg was removed using a chemical depilatory. Readings were taken using the
543 probe from at least 10 different spots on the TA muscle. The AU was determined as the average
544 AU value during a plateau phase of each measurement.
545
546 **RNA and genomic DNA isolation and qPCR**

547 Cultured cells were washed with ice cold PBS and lysed on the place with Trizol™. RNA was
548 isolated using the DirectZol™ RNA Microprep Kit (Zymo Research, R2062) with on-column
549 DNase digestion followed by cDNA synthesis using the Transcriptor First Strand cDNA
550 synthesis kit (Roche Molecular Diagnostics, 04379012001) using random primers. Genomic
551 DNA for genotyping was isolated from mouse tail snips with lysis buffer containing Proteinase
552 K (Sigma-Aldrich, P2308). qPCR was performed using GoTaq qPCR Master Mix (Promega,
553 A6002). The input RNA amount was normalized across all samples and *18S rRNA* or *HtatsF1*
554 was used for normalization of qPCR across samples. Primer sequences are listed in Table S3. All
555 primers were synthesized as custom DNA oligos from Integrated DNA technologies (IDT).
556

557 **Single cell RNAsequencing and analysis**

558 Cells for single cell RNAseq were obtained from hind limb muscles of 2-3 moth-old
559 *Pax7$^{tdT}$:Flk1$^{GFP}$* mice following enzymatic digestion as previously described (Liu et al., 2015).
560 Dead cells were excluded from the analysis using ZombieNIR (Biolegends, 423105).
561 TdTomato(+) and GFP(+) cells were sorted individually and then 20% of GFP(+) cells were
562 spiked into 80% tdTomato(+). We loaded ~5,000 cells into 1 channel of the Chromium system
563 for each of these samples and prepared libraries according to the manufacturer's protocol using
564 version 2.0 chemistry (10x Genomics). Following capture and lysis, we synthesized cDNA and
565 amplified for 12 cycles as per the manufacturer's protocol (10x Genomics). The amplified cDNA
566 was used to construct Illumina sequencing libraries that were each sequenced with ~300K
567 read/cell on one lane of an Illumina HiSeq 2500 machine. We used Cell Ranger 3.1 (10X
568 Genomics) to process raw sequencing data. For A custom genome was constructed to include
569 *eGFP-SV40*, *tdTomato-WPRE-BGHPolyA* and *Pax7-IRES-CreERT2* transgenes. Detailed step-

570 by-step instructions can be found at https://github.com/verma014/10XCustomRef. We carried
571 out analyses of the filtered data using Seurat suite version 3.0 (Stuart et al., 2019) in R studio
572 (RStudio Team, 2020). For cell imputation, we utilized ALRA through the Seurat wrapper with
573 default settings(Linderman et al., 2018). Additional scRNAseq datasets were obtained from GEO
574 and analyzed using the same method as listed above. A myogenic score was calculated based on
575 the expression of *Myog*, *Pax7*, *Myod1* and *Myf5*. Step-by-step instructions for the analysis can be
576 found on https://github.com/verma014/10XCustomRef.
577

578 **Background Subtraction**

579 10x Genomics scRNAseq platform uses many more droplets than cells and so following a run,
580 there are many droplets that do not have cells. These droplets still get sequenced with some of
581 the RNA that is in the solution. This floating RNA can be used to estimate the "background" in
582 each droplet. A better description of this can be found by the developers of 'SoupX' (Young and
583 Behjati, 2020). Since *Cdh5* expression has previously been verified in MuSCs using RNAscope,
584 we were able to use it as a positive control to remove the background or "soup" from our data. If
585 *Cdh5* is absent from MuSC, we know that the background subtraction was too aggressive and
586 that subtracting the Soup is not reliable in our case. In addition, we know certain genes that are
587 considered to be specific for MuSCs, muscle ECs or muscle fibers based on the bulk RNAseq
588 (Verma et al., 2018). The top 5 genes that are specific to these population (and also detected by
589 10x) were selected and used to show the background in our data set was 14.40% and 13.89% for
590 the D0 and D3 dataset, respectively. The step-by-step instructions can be found on
591 https://github.com/verma014/10XCustomRef.
592

593 **Bulk RNAseq and Microarray Analysis**

594 FASTQ files were downloaded from SRA using SRA-toolkit. Sequences were trimmed using
595 trimmomatic to remove adapter contamination and low-quality reads. Trimmed sequences were
596 mapped to mouse mm10 using Hisat2 (Pertea et al., 2016). Transcript assembly was performed
597 using StringTie (Pertea et al., 2016). Cell type specificity was determined as previously
598 described (Verma et al., 2018). Microarray analysis was performed using the Affymetrix
599 Transcriptome Analysis Console (TAC). Samples in each experiment were RNA normalized and
600 the expression was acquired using the Affeymetrix Expression analysis console with gene level
601 expression. Heatmaps were generated in Prism 9 (Graphpad, La Jolla, CA). The code for
602 generating each graph is listed in the following table, along with the link to the data in tabular
603 format.

604

605 **Quantification and Statistical Analysis**

606 Statistical analysis was performed using Prism 9 (Graphpad, La Jolla, CA) or RStudio (RStudio
607 Team, 2020). For comparison between two groups, an unpaired T-test was used. For comparison
608 between multiple groups, a one-way ANOVA was used with multiple comparisons to the control.
609 Distributions were compared using a chi-squared test. Graphing of the data was performed using
610 Prism 9. Vector diagrams were modified using Graphic (Autodesk). All values are means ±SEM
611 unless noted otherwise. * indicates $p < 0.05$, ** indicates $p < 0.01$, *** indicates $p < 0.001$.

612

613 **Data and Software Availability**

614 All the data was obtained from NCBI GEO. Microarrays of mouse MuSCs were obtained from
615 GSE3483 (Fukada et al., 2007). scRNAseq of MuSCs and muscle ECs was performed in this

616 study (GSE129057). scRNAseq of whole muscle was obtained from GSE143437 (De Micheli et
617 al., 2020). Bulk RNAseq of MuSCs, ECs and single muscle fibers was obtained from
618 GSE108739 (Verma et al., 2018) and GSE64379 (Ryall et al., 2015). Bulk RNAseq of TU-
619 tagged RNA of MuSCs was obtianed from GSE97399 (van Velthoven et al., 2017). Bulk
620 RNAseq of fixed and unfixed MuSCs was obtained from GSE113631 (Yue et al., 2020).
621 Exercise, ALS, DMD, BMD, FSHD GSE3307, Early DMD GSE465, *mdx* GSE466, GRMD
622 GSE69040, Satellite cells GSE15155. All arrays were normalized to their respective controls. All
623 arrays and RNAseq data are listed in Supplemental Table 1 (Table S1).
624

625 **Acknowledgements**

626 We thank Minnesota Supercomputing Institute, University of Minnesota Imaging Center,
627 University of Minnesota FACS Facility, and University of Minnesota Genomics Center for
628 providing data for this paper. We also thank Jake Trask for critical reading of this paper. We
629 thank Drs. Yosuke Mukouyama (National Institute of Health), Napoleone Ferrara (Genentech),
630 Guo-Hua Fong (University of Connecticut) and Masatsugu Ema (Siga University of Medical
631 Science) for providing *VEGFA*$^{LoxP/LoxP}$, *Flt1*$^{LoxP/LoxP}$ and *Flk1-GFP* mice, respectively. This work
632 was supported by NIHT32-GM008244 and NIHF30AR066454 to MV, NIAMS grant AR070231
633 to RSK, a fellowship of the Training Program in Stem Cell Research from the New York State
634 Department of Health to A.P.K. (NYSTEM-C32561GG) and NIHR01AR062142,
635 NIHR21AR070319, MDA Research Grant, and Regenerative Medicine Minnesota (RMM) Grant
636 to AA.

637

638 **Competing interests**

639 The authors declare no competing interests.

640

641 **Reference**

642 Aartsma-Rus A, van Putten M. 2014. Assessing Functional Performance in the Mdx Mouse
643 Model. *J Vis Exp*. 51303. doi:10.3791/51303

644 Arsic N, Zacchigna S, Zentilin L, Ramirez-Correa G, Pattarini L, Salvi A, Sinagra G, Giacca M.
645 2004. Vascular endothelial growth factor stimulates skeletal muscle regeneration in vivo.
646 *Mol Ther* **10**:844–854. doi: 10.1016/j.ymthe.2004.08.007

647 Asakura A, Komaki M, Rudnicki M. 2001. Muscle satellite cells are multipotential stem cells
648 that exhibit myogenic, osteogenic, and adipogenic differentiation. *Differentiation* **68**:245–
649 253. doi: 10.1046/j.1432-0436.2001.680412.x.

650 Asakura A, Seale P, Girgis-Gabardo A, Rudnicki MA. 2002. Myogenic specification of side
651 population cells in skeletal muscle. *J Cell Biol* **159**:123–134. doi: 10.1083/jcb.200202092.

652 Bae DG, Kim TD, Li G, Yoon WH, Chae CB. 2005. Anti-flt1 peptide, a vascular endothelial
653 growth factor receptor 1-specific hexapeptide, inhibits tumor growth and metastasis. *Clin*
654 *Cancer Res* **11**:2651–2661. doi: 10.1158/1078-0432.CCR-04-1564

655 Bakay M, Wang Z, Melcon G, Schiltz L, Xuan J, Zhao P, Sartorelli V, Seo J, Pegoraro E,
656 Angelini C, Shneiderman B, Escolar D, Chen Y-W, Winokur ST, Pachman LM, Fan C,
657 Mandler R, Nevo Y, Gordon E, Zhu Y, Dong Y, Wang Y, Hoffman EP. 2006. Nuclear
658 envelope dystrophies show a transcriptional fingerprint suggesting disruption of Rb-MyoD
659 pathways in muscle regeneration. *Brain* **129**:996–1013. doi:10.1093/brain/awl023

660 Bosco J, Zhou Z, Gabriëls S, Verma M, Liu N, Miller BK, Gu S, Lundberg DM, Huang Y,
661 Brown E, Josiah S, Meiyappan M, Traylor MJ, Chen N, Asakura A, De Jonge N, Blanchetot
662 C, de Haard H, Duffy HS, Keefe D. 2021. VEGFR-1/Flt-1 inhibition increases
663 angiogenesis and improves muscle function in a mouse model of Duchenne muscular

664 dystrophy. *Mol Ther Methods Clin Dev* **23**:21:369-381. doi: 10.1016/j.omtm.2021.03.013

665 Bouchentouf M, Benabdallah BF, Bigey P, Yau TM, Scherman D, Tremblay JP. 2008. Vascular
666 endothelial growth factor reduced hypoxia-induced death of human myoblasts and
667 improved their engraftment in mouse muscles. *Gene Ther* **15**:404–414.
668 doi: 10.1038/sj.gt.3303059

669 Bryan BA, Walshe TE, Mitchell DC, Havumaki JS, Saint-Geniez M, Maharaj AS, Maldonado
670 AE, D'Amore PA, Bryan BA, Walshe TE, Mitchell DC, Havumaki JS, Saint-Geniez M,
671 Maharaj AS, Maldonado AE, D'Amore PA. 2008. Coordinated vascular endothelial growth
672 factor expression and signaling during skeletal myogenic differentiation. *Mol Biol Cell*
673 **19**:994–1006. doi:10.1091/mbc.E07-09-0856

674 Chapman VM, Miller DR, Armstrong D, Caskey CT. 1989. Recovery of induced mutations for
675 X chromosome-linked muscular dystrophy in mice. *Proc Natl Acad Sci U S A* **86**:1292-6.
676 doi: 10.1073/pnas.86.4.1292

677 Charville GW, Cheung TH, Yoo B, Santos PJ, Lee GK, Shrager JB, Rando TA. 2015. Ex Vivo
678 Expansion and In Vivo Self-Renewal of Human Muscle Stem Cells. *Stem cell Reports*
679 **5**:621–32. doi:10.1016/j.stemcr.2015.08.004

680 Chen YW, Zhao P, Borup R, Hoffman EP. 2000. Expression profiling in the muscular
681 dystrophies: identification of novel aspects of molecular pathophysiology. *J Cell Biol*
682 **151**:1321–36. doi:10.1083/jcb.151.6.1321

683 Chestnut B, Casie Chetty S, Koenig AL, Sumanas S. 2020. Single-cell transcriptomic analysis
684 identifies the conversion of zebrafish Etv2-deficient vascular progenitors into skeletal
685 muscle. *Nat Commun* **11**:2796. doi:10.1038/s41467-020-16515-y

686 Christov C, Chretien F, Abou-Khalil R, Bassez G, Vallet G, Authier FJ, Bassaglia Y, Shinin V,

687 Tajbakhsh S, Chazaud B, Gherardi RK. 2007. Muscle satellite cells and endothelial cells:
688 close neighbors and privileged partners. *Mol Biol Cell* **18**:1397–1409.
689 doi: 10.1091/mbc.e06-08-0693
690 De Angelis L, Berghella L, Coletta M, Lattanzi L, Zanchi M, Cusella-De Angelis MG, Ponzetto
691 C, Cossu G. 1999. Skeletal myogenic progenitors originating from embryonic dorsal aorta
692 coexpress endothelial and myogenic markers and contribute to postnatal muscle growth and
693 regeneration. *J Cell Biol* **147**:869–877. doi:10.1083/jcb.147.4.869
694 De Micheli AJ, Laurilliard EJ, Heinke CL, Ravichandran H, Fraczek P, Soueid-Baumgarten S,
695 De Vlaminck I, Elemento O, Cosgrove BD. 2020. Single-Cell Analysis of the Muscle Stem
696 Cell Hierarchy Identifies Heterotypic Communication Signals Involved in Skeletal Muscle
697 Regeneration. *Cell Rep* **30**:3583-3595.e5. doi:10.1016/j.celrep.2020.02.067
698 Delavar H, Nogueira L, Wagner PD, Hogan MC, Metzger D, Breen EC. 2014. Skeletal myofiber
699 VEGF is essential for the exercise training response in adult mice. *AJP Regul Integr Comp*
700 *Physiol* **306**:R586–R595. doi:10.1152/ajpregu.00522.2013
701 Desrochers LM, Antonyak MA, Cerione RA. 2016. Extracellular Vesicles: Satellites of
702 Information Transfer in Cancer and Stem Cell Biology. *Dev Cell* **37**:301-309. doi:
703 10.1016/j.devcel.2016.04.019.
704 Domigan CK, Warren CM, Antanesian V, Happel K, Ziyad S, Lee S, Krall A, Duan L, Torres-
705 Collado AX, Castellani LW, Elashoff D, Christofk HR, van der Bliek AM, Potente M,
706 Iruela-Arispe ML. 2015. Autocrine VEGF maintains endothelial survival through regulation
707 of metabolism and autophagy. *J Cell Sci* **128**:2236–48. doi:10.1242/jcs.163774
708 Drummond CJ, Hatley ME. 2018. A Case of mistaken identity: Rhabdomyosarcoma
709 development from endothelial progenitor cells. *Mol Cell Oncol* **5**:e1448246.

710 doi:10.1080/23723556.2018.1448246

711 Eichmann A, Marcelle C, Bréant C, Le Douarin NM. 1993. Two molecules related to the VEGF
712 receptor are expressed in early endothelial cells during avian embryonic development. *Mech*
713 *Dev* **42**:33–48. doi:10.1016/0925-4773(93)90096-g

714 Ema M, Takahashi S, Rossant J. 2006. Deletion of the selection cassette, but not cis-acting
715 elements, in targeted Flk1-lacZ allele reveals Flk1 expression in multipotent mesodermal
716 progenitors. *Blood* **107**:111–7. doi:10.1182/blood-2005-05-1970

717 Esner M, Meilhac SM, Relaix F, Nicolas J-F, Cossu G, Buckingham ME. 2006. Smooth muscle
718 of the dorsal aorta shares a common clonal origin with skeletal muscle of the myotome.
719 *Development* **133**:737–49. doi:10.1242/dev.02226

720 Fukada S, Uezumi A, Ikemoto M, Masuda S, Segawa M, Tanimura N, Yamamoto H, Miyagoe-
721 Suzuki Y, Takeda S. 2007. Molecular signature of quiescent satellite cells in adult skeletal
722 muscle. *Stem Cells* **25**:2448–59. doi:10.1634/stemcells.2007-0019

723 Gay L, Miller MR, Ventura PB, Devasthali V, Vue Z, Thompson HL, Temple S, Zong H, Cleary
724 MD, Stankunas K, Doe CQ. 2013. Mouse TU tagging: a chemical/genetic intersectional
725 method for purifying cell type-specific nascent RNA. *Genes Dev* **27**:98–115.
726 doi:10.1101/gad.205278.112

727 Gerber HP, McMurtrey A, Kowalski J, Yan M, Keyt B a, Dixit V, Ferrara N. 1998. Vascular
728 endothelial growth factor regulates endothelial cell survival through the
729 phosphatidylinositol 3'-kinase/Akt signal transduction pathway. Requirement for Flk-
730 1/KDR activation. *J Biol Chem* **273**:30336–43. doi : 10.1074/jbc.273.46.30336

731 Germani A, Di Carlo A, Mangoni A, Straino S, Giacinti C, Turrini P, Biglioli P, Capogrossi MC.
732 2003. Vascular endothelial growth factor modulates skeletal myoblast function. *Am J*

733 *Pathol* **163**:1417–1428. doi: 10.1016/S0002-9440(10)63499-2

734 Giordani L, He GJ, Negroni E, Sakai H, Law JYC, Siu MM, Wan R, Corneau A, Tajbakhsh S,
735 Cheung TH, Le Grand F. 2018. High-Dimensional Single-Cell Cartography Reveals Novel
736 Skeletal Muscle-Resident Cell Populations. *Mol Cell* **74**:609-621.e6. doi:
737 10.1016/j.molcel.2019.02.026.

738 Goel AJ, Rieder MK, Arnold HH, Radice GL, Krauss RS. 2017. Niche Cadherins Control the
739 Quiescence-to-Activation Transition in Muscle Stem Cells. *Cell Rep* **21**:2236–2250.
740 doi:10.1016/j.celrep.2017.10.102

741 Hardy D, Besnard A, Latil M, Jouvion G, Briand D, Thépenier C, Pascal Q, Guguin A, Gayraud-
742 Morel B, Cavaillon J-M, Tajbakhsh S, Rocheteau P, Chrétien F. 2016. Comparative Study
743 of Injury Models for Studying Muscle Regeneration in Mice. *PLoS One* **11**:e0147198.
744 doi:10.1371/journal.pone.0147198

745 Hirai H, Verma M, Watanabe S, Tastad C, Asakura Y, Asakura A. 2010. MyoD regulates
746 apoptosis of myoblasts through microRNA-mediated down-regulation of Pax3. *J Cell Biol*
747 **191**:347–65. doi:10.1083/jcb.201006025

748 Ho VC, Duan L-J, Cronin C, Liang BT, Fong G-H. 2012. Elevated vascular endothelial growth
749 factor receptor-2 abundance contributes to increased angiogenesis in vascular endothelial
750 growth factor receptor-1-deficient mice. *Circulation* **126**:741–52.
751 doi:10.1161/CIRCULATIONAHA.112.091603

752 Huang P, Schulz TJ, Beauvais A, Tseng YH, Gussoni E. 2014.
753 Intramuscular adipogenesis is inhibited by myo-endothelial progenitors with functioning
754 Bmpr1a signalling. *Nat Commun* **5**:4063. doi: 10.1038/ncomms5063.

755 Hutcheson DA, Kardon G. 2009. Genetic manipulations reveal dynamic cell and gene functions:

756 Cre-ating a new view of myogenesis. *Cell Cycle* **8**:3675–8. doi:10.4161/cc.8.22.9992

757 Kann AP, Krauss RS. 2019. Multiplexed RNAscope and immunofluorescence on whole-mount
758 skeletal myofibers and their associated stem cells. *Development* **146**:dev179259
759 doi:10.1242/dev.179259

760 Kardon G, Campbell JK, Tabin CJ. 2002. Local extrinsic signals determine muscle and
761 endothelial cell fate and patterning in the vertebrate limb. *Dev Cell* **3**:533–45.
762 doi:10.1016/s1534-5807(02)00291-5

763 Keifer OP, O'Connor DM, Boulis NM. 2014. Gene and protein therapies utilizing VEGF for
764 ALS. *Pharmacol Ther* **141**:261–71. doi:10.1016/j.pharmthera.2013.10.009

765 Kobayashi H, Butler JM, O'Donnell R, Kobayashi M, Ding B-S, Bonner B, Chiu VK, Nolan DJ,
766 Shido K, Benjamin L, Rafii S. 2010. Angiocrine factors from Akt-activated endothelial cells
767 balance self-renewal and differentiation of haematopoietic stem cells. *Nat Cell Biol*
768 **12**:1046–56. doi:10.1038/ncb2108

769 Kodippili K, Thorne PK, Laughlin MH, Duan D. 2021. Dystrophin deficiency impairs vascular
770 structure and function in the canine model of Duchenne muscular dystrophy. *J Pathol*
771 **254**:589-605. doi:10.1002/path.5704

772 Lagha M, Brunelli S, Messina G, Cumano A, Kume T, Relaix F, Buckingham ME. 2009.
773 Pax3:Foxc2 reciprocal repression in the somite modulates muscular versus vascular cell fate
774 choice in multipotent progenitors. *Dev Cell* **17**:892–9. doi:10.1016/j.devcel.2009.10.021

775 Latroche C, Matot B, Martins-Bach A, Briand D, Chazaud B, Wary C, Carlier PG, Chrétien F,
776 Jouvion G. 2015. Structural and Functional Alterations of Skeletal Muscle Microvasculature
777 in Dystrophin-Deficient mdx Mice. *Am J Pathol* **185**:2482-94.
778 doi:10.1016/j.ajpath.2015.05.009

779 Latroche C, Weiss-Gayet M, Muller L, Gitiaux C, Leblanc P, Liot S, Ben-Larbi S, Abou-Khalil
780 R, Verger N, Bardot P, Magnan M, Chrétien F, Mounier R, Germain S, Chazaud B. 2017.
781 Coupling between Myogenesis and Angiogenesis during Skeletal Muscle Regeneration Is
782 Stimulated by Restorative Macrophages. *Stem Cell Reports* **9**:2018-2033.
783 doi:10.1016/j.stemcr.2017.10.027
784 Le Grand F, Auda-Boucher G, Levitsky D, Rouaud T, Fontaine-Pérus J, Gardahaut M-F. 2004.
785 Endothelial cells within embryonic skeletal muscles: a potential source of myogenic
786 progenitors. *Exp Cell Res* **301**:232–41. doi:10.1016/j.yexcr.2004.07.028
787 Lee S, Chen TT, Barber CL, Jordan MC, Murdock J, Desai S, Ferrara N, Nagy A, Roos KP,
788 Iruela-Arispe ML. 2007. Autocrine VEGF signaling is required for vascular homeostasis.
789 *Cell* **130**:691–703. doi:10.1016/j.cell.2007.06.054
790 Li Y, Zhang F, Nagai N, Tang Z, Zhang S, Scotney P, Lennartsson J, Zhu C, Qu Y, Fang C, Hua
791 J, Matsuo O, Fong GH, Ding H, Cao Y, Becker KG, Nash A, Heldin CH, Li X. 2008.
792 VEGF-B inhibits apoptosis via VEGFR-1-mediated suppression of the expression of BH3-
793 only protein genes in mice and rats. *J Clin Invest* **118**:913–923. doi:10.1172/JCI33673
794 Linderman GC, Zhao J, Kluger Y. 2018. Zero-preserving imputation of scRNA-seq data using
795 low-rank approximation. *bioRxiv* 397588. doi**:** https://doi.org/10.1101/397588
796 Liu L, Cheung TH, Charville GW, Rando T a. 2015. Isolation of skeletal muscle stem cells by
797 fluorescence-activated cell sorting. *Nat Protoc* **10**:1612–1624. doi:10.1038/nprot.2015.110
798 Liu Y, Berendsen AD, Jia S, Lotinun S, Baron R, Ferrara N, Olsen BR. 2012. Intracellular
799 VEGF regulates the balance between osteoblast and adipocyte differentiation. *J Clin Invest*
800 **122**:3101–3113. doi:10.1172/JCI61209
801 Loiben AM, Soueid-Baumgarten S, Kopyto RF, Bhattacharya D, Kim JC, Cosgrove BD. 2017.

802 Data-Modeling Identifies Conflicting Signaling Axes Governing Myoblast Proliferation and
803 Differentiation Responses to Diverse Ligand Stimuli. *Cell Mol Bioeng* **10**:433–450.
804 doi:10.1007/s12195-017-0508-5
805 Mac Gabhann F, Qutub AA, Annex BH, Popel AS. 2011. Systems biology of pro-angiogenic
806 therapies targeting the VEGF system. *Wiley Interdiscip Rev Syst Biol Med* **2**:694–707.
807 doi:10.1002/wsbm.92
808 Madisen L, Zwingman TA, Sunkin SM, Oh SW, Zariwala HA, Gu H, Ng LL, Palmiter RD,
809 Hawrylycz MJ, Jones AR, Lein ES, Zeng H. 2010. A robust and high-
810 throughput Cre reporting and characterization system for the whole mouse brain. *Nat*
811 *Neurosci* **13**:133-40. doi: 10.1038/nn.2467. Epub 2009 Dec 20
812 Mayeuf-Louchart A, Lagha M, Danckaert A, Rocancourt D, Relaix F, Vincent SD, Buckingham
813 M. 2014. Notch regulation of myogenic versus endothelial fates of cells that migrate from
814 the somite to the limb. *Proc Natl Acad Sci U S A* **111**:8844–8849.
815 doi:10.1073/pnas.1407606111
816 Mayeuf-Louchart A, Montarras D, Bodin C, Kume T, Vincent SD, Buckingham M. 2016.
817 Endothelial cell specification in the somite is compromised in Pax3-positive progenitors of
818 Foxc1/2 conditional mutants, with loss of forelimb myogenesis. *Development* **143**:872–9.
819 doi:10.1242/dev.128017
820 Mercatelli N, Dimauro I, Ciafré SA, Farace MG, Caporossi D. 2010. AlphaB-crystallin is
821 involved in oxidative stress protection determined by VEGF in skeletal myoblasts. *Free*
822 *Radic Biol Med* **49**:374–82. doi:10.1016/j.freeradbiomed.2010.04.027
823 Messina S, Mazzeo A, Bitto A, Aguennouz M, Migliorato A, De Pasquale MG, Minutoli L,
824 Altavilla D, Zentilin L, Giacca M, Squadrito F, Vita G. 2007. VEGF overexpression via

825 adeno-associated virus gene transfer promotes skeletal muscle regeneration and enhances
826 muscle function in mdx mice. *FASEB J* **21**:3737–3746. doi : 10.1096/fj.07-8459com
827 Minasi MG, Riminucci M, De Angelis L, Borello U, Berarducci B, Innocenzi A, Caprioli A,
828 Sirabella D, Baiocchi M, De Maria R, Boratto R, Jaffredo T, Broccoli V, Bianco P, Cossu G.
829 2002. The meso-angioblast: a multipotent, self-renewing cell that originates from the dorsal
830 aorta and differentiates into most mesodermal tissues. *Development* **129**:2773–83. doi:
831 10.1242/dev.129.11.2773
832 Miquerol L, Gertsenstein M, Harpal K, Rossant J, Nagy a. 1999. Multiple developmental roles
833 of VEGF suggested by a LacZ-tagged allele. *Dev Biol* **212**:307–322.
834 doi:10.1006/dbio.1999.9355
835 Motohashi N, Asakura A. 2014. Muscle satellite cell heterogeneity and self-renewal. *Front Cell*
836 *Dev Biol* **2**:1–11. doi:10.3389/fcell.2014.00001
837 Motohashi N, Asakura Y, Asakura A. 2014. Isolation, culture, and transplantation of muscle
838 satellite cells. *J Vis Exp* 50846. doi:10.3791/50846
839 Motoike T, Markham DW, Rossant J, Sato TN. 2003. Evidence for novel fate of Flk1+
840 progenitor: contribution to muscle lineage. *Genesis* **35**:153–9. doi:10.1002/gene.10175
841 Murach KA, Vechetti IJ, Van Pelt DW, Crow SE, Dungan CM, Figueiredo VC, Kosmac K, Fu X,
842 Richards CI, Fry CS, McCarthy JJ, Peterson CA. 2020. Fusion-Independent Satellite Cell
843 Communication to Muscle Fibers During Load-Induced Hypertrophy. *Function* **1**:1–15.
844 doi:10.1093/function/zqaa009
845 Murphy MM, Lawson J a, Mathew SJ, Hutcheson D a, Kardon G. 2011. Satellite cells,
846 connective tissue fibroblasts and their interactions are crucial for muscle regeneration. *J*
847 *Cell Sci* **124**:e1–e1. doi:10.1242/jcs098228

848 Noren DP, Chou WH, Lee SH, Qutub AA, Warmflash A, Wagner DS, Popel AS, Levchenko A.
849 2016. Endothelial cells decode VEGF-mediated Ca2+ signaling patterns to produce distinct
850 functional responses. *Sci Signal* **9**:ra20–ra20. doi:10.1126/scisignal.aad3188
851 Okabe K, Kobayashi S, Yamada T, Kurihara T, Tai-nagara I. 2014. Neurons Limit Angiogenesis
852 by Titrating VEGF in Retina. *Cell* **159**:584–596. doi:10.1016/j.cell.2014.09.025
853 Olfert IM, Howlett RA, Tang K, Dalton ND, Gu Y, Peterson KL, Wagner PD, Breen EC. 2009.
854 Muscle-specific VEGF deficiency greatly reduces exercise endurance in mice. *J Physiol*
855 **587**:1755–1767. doi: : 10.1113/jphysiol.2008.164384
856 Pallafacchina G, François S, Regnault B, Czarny B, Dive V, Cumano A, Montarras D,
857 Buckingham M. 2010. An adult tissue-specific stem cell in its niche: a gene profiling
858 analysis of in vivo quiescent and activated muscle satellite cells. *Stem Cell Res* **4**:77–91.
859 doi:10.1016/j.scr.2009.10.003
860 Pertea M, Kim D, Pertea GM, Leek JT, Salzberg SL. 2016. Transcript-level expression analysis
861 of RNA-seq experiments with HISAT, StringTie and Ballgown. *Nat Protoc* **11**:1650–1667.
862 doi:10.1038/nprot.2016.095
863 Podkalicka P, Mucha O, Kaziród K, Bronisz-Budzyńska I, Ostrowska-Paton S, Tomczyk M,
864 Andrysiak K, Stępniewski J, Dulak J, Łoboda A. 2021. Age-Dependent Dysregulation of
865 Muscle Vasculature and Blood Flow Recovery after Hindlimb Ischemia in the mdx Model
866 of Duchenne Muscular Dystrophy. *Biomedicines* **9**:481. doi: 10.3390/biomedicines9050481.
867 Poesen K, Lambrechts D, Van Damme P, Dhondt J, Bender F, Frank N, Bogaert E, Claes B,
868 Heylen L, Verheyen A, Raes K, Tjwa M, Eriksson U, Shibuya M, Nuydens R, Van Den
869 Bosch L, Meert T, D'Hooge R, Sendtner M, Robberecht W, Carmeliet P. 2008. Novel Role
870 for Vascular Endothelial Growth Factor (VEGF) Receptor-1 and Its Ligand VEGF-B in

871 Motor Neuron Degeneration. *J Neurosci* **28**:10451–10459. doi:10.1523/JNEUROSCI.1092-
872 08.2008
873 Roobrouck VD, Clavel C, Jacobs SA, Ulloa-Montoya F, Crippa S, Sohni A, Roberts SJ, Luyten
874 FP, Van Gool SW, Sampaolesi M, Delforge M, Luttun A, Verfaillie CM. 2011.
875 Differentiation potential of human postnatal mesenchymal stem cells, mesoangioblasts, and
876 multipotent adult progenitor cells reflected in their transcriptome and partially influenced by
877 the culture conditions. *Stem Cells* **29**:871–82. doi:10.1002/stem.633
878 RStudio Team. 2020. RStudio: Integrated Development for R. RStudio, PBC, Boston, MA.
879 http://www.rstudio.com/
880 Ryall JG, Dell'Orso S, Derfoul A, Juan A, Zare H, Feng X, Clermont D, Koulnis M, Gutierrez-
881 Cruz G, Fulco M, Sartorelli V. 2015. The NAD+-dependent sirt1 deacetylase translates a
882 metabolic switch into regulatory epigenetics in skeletal muscle stem cells. *Cell Stem Cell*
883 **16**:171–183. doi:10.1016/j.stem.2014.12.004
884 Sakurai H, Okawa Y, Inami Y, Nishio N, Isobe K. 2008. Paraxial mesodermal progenitors
885 derived from mouse embryonic stem cells contribute to muscle regeneration via
886 differentiation into muscle satellite cells. *Stem Cells* **26**:1865–73.
887 doi:10.1634/stemcells.2008-0173
888 Schindelin J, Arganda-Carreras I, Frise E, Kaynig V, Longair M, Pietzsch T, Preibisch S,
889 Rueden C, Saalfeld S, Schmid B, Tinevez J-Y, White DJ, Hartenstein V, Eliceiri K,
890 Tomancak P, Cardona A. 2012. Fiji: an open-source platform for biological-image analysis.
891 *Nat Methods* **9**:676–82. doi:10.1038/nmeth.2019
892 Shimizu-Motohashi Y, Asakura Y, Motohashi N, Belur NR, Baumrucker MG, Asakura A. 2015.
893 Pregnancy-induced amelioration of muscular dystrophy phenotype in mdx mice via muscle

894 membrane stabilization effect of glucocorticoid. *PLoS One*. **10**:e0120325. doi:
895 10.1371/journal.pone.0120325.
896 Stuart T, Butler A, Hoffman P, Hafemeister C, Papalexi E, Mauck WM, Hao Y, Stoeckius M,
897 Smibert P, Satija R. 2019. Comprehensive Integration of Single-Cell Data. *Cell* **177**:1888-
898 1902.e21. doi:10.1016/j.cell.2019.05.031
899 Tamaki T, Akatsuka A, Ando K, Nakamura Y, Matsuzawa H, Hotta T, Roy RR, Edgerton VR.
900 2002. Identification of myogenic-endothelial progenitor cells in the interstitial spaces of
901 skeletal muscle. *J Cell Biol* **157**:571–7. doi:10.1083/jcb.200112106
902 Tang K, Breen EC, Gerber H-P, Ferrara NM a, Wagner PD. 2004. Capillary regression in
903 vascular endothelial growth factor-deficient skeletal muscle. *Physiol Genomics* **18**:63–69.
904 doi:10.1152/physiolgenomics.00023.2004
905 Torre E, Dueck H, Shaffer S, Gospocic J, Gupte R, Bonasio R, Kim J, Murray J, Raj A. 2018.
906 Rare Cell Detection by Single-Cell RNA Sequencing as Guided by Single-Molecule RNA
907 FISH. *Cell Syst* **6**:171-179.e5. doi:10.1016/j.cels.2018.01.014
908 Tozer S, Bonnin M-A, Relaix F, Di Savino S, García-Villalba P, Coumailleau P, Duprez D. 2007.
909 Involvement of vessels and PDGFB in muscle splitting during chick limb development.
910 *Development* **134**:2579–91. doi:10.1242/dev.02867
911 Tseng BS, Zhao P, Pattison JS, Gordon SE, Granchelli JA, Madsen RW, Folk LC, Hoffman EP,
912 Booth FW. 2002. Regenerated mdx mouse skeletal muscle shows differential mRNA
913 expression. *J Appl Physiol* **93**:537–45. doi:10.1152/japplphysiol.00202.2002
914 Turaç G, Hindley CJ, Thomas R, Davis JA, Deleidi M, Karaöz E, Pruszak J. 2013. Combined
915 Flow Cytometric Analysis of Surface and Intracellular Antigens Reveals Surface Molecule
916 Markers of Human Neuropoiesis. *PLoS One* **8**:1–14. doi:10.1371/journal.pone.0068519

917 van Velthoven CTJ, de Morree A, Egner IM, Brett JO, Rando TA. 2017. Transcriptional
918 Profiling of Quiescent Muscle Stem Cells In Vivo. *Cell Rep* **21**:1994–2004.
919 doi:10.1016/j.celrep.2017.10.037
920 Veldman MB, Zhao C, Gomez G a, Lindgren AG, Huang H, Yang H, Yao S, Martin BL,
921 Kimelman D, Lin S. 2013. Transdifferentiation of fast skeletal muscle into functional
922 endothelium in vivo by transcription factor etv2. *PLoS Biol* **11**:e1001590.
923 doi:10.1371/journal.pbio.1001590
924 Vempati P, Popel AS, Mac Gabhann F. 2014. Extracellular regulation of VEGF: Isoforms,
925 proteolysis, and vascular patterning. *Cytokine Growth Factor Rev* **25**:1–19.
926 doi:10.1016/j.cytogfr.2013.11.002
927 Verma M, Asakura Y, Hirai H, Watanabe S, Tastad C, Fong G-H, Ema M, Call JA, Lowe DA,
928 Asakura A. 2010. Flt-1 haploinsufficiency ameliorates muscular dystrophy phenotype by
929 developmentally increased vasculature in mdx mice. *Hum Mol Genet* **19**:4145–59.
930 doi:10.1093/hmg/ddq334
931 Verma M, Asakura Y, Murakonda BSR, Pengo T, Latroche C, Chazaud B, McLoon LK,
932 Asakura A. 2018. Muscle Satellite Cell Cross-Talk with a Vascular Niche Maintains
933 Quiescence via VEGF and Notch Signaling. *Cell Stem Cell* **23**:530-543.e9.
934 doi:10.1016/j.stem.2018.09.007
935 Verma M, Shimizu-Motohashi Y, Asakura Y, Ennen JP, Bosco J, Zhou Z, Fong G, Josiah S,
936 Keefe D, Asakura A. 2019. Inhibition of FLT1 ameliorates muscular dystrophy phenotype
937 by increased vasculature in a mouse model of Duchenne muscular dystrophy. *PLOS Genet*
938 **15**:e1008468. doi:10.1371/journal.pgen.1008468
939 Vieira NM, Elvers I, Alexander MS, Moreira YB, Eran A, Gomes JP, Marshall JL, Karlsson EK,

940 Verjovski-Almeida S, Lindblad-Toh K, Kunkel LM, Zatz M. 2015. Jagged 1 Rescues the
941 Duchenne Muscular Dystrophy Phenotype. *Cell* **163**:1204–1213.
942 doi:10.1016/j.cell.2015.10.049
943 Wagner PD, Olfert IM, Tang K, Breen EC. 2006. Muscle-targeted deletion of VEGF and
944 exercise capacity in mice. *Respir Physiol Neurobiol* **151**:159–166.
945 doi:10.1016/j.resp.2005.09.007
946 Wang C, Liu W, Nie Y, Qaher M, Horton HE, Yue F, Asakura A, Kuang S. 2017. Loss of MyoD
947 Promotes Fate Transdifferentiation of Myoblasts Into Brown Adipocytes. *EBioMedicine*
948 **16**:212-223. doi: 10.1016/j.ebiom.2017.01.015.
949 Xin C, Chu X, Wei W, Kuang B, Wang Y, Tang Y, Chen J, You H, Li C, Wang B. 2021.
950 Combined gene therapy via VEGF and mini-dystrophin synergistically improves
951 pathologies in temporalis muscle of dystrophin/utrophin double knockout mice. *Hum Mol*
952 *Genet* **30**:1349-1359. doi: 10.1093/hmg/ddab120.
953 Yan G, Yan R, Chen C, Chen C, Zhao Y, Qin W, Veldman MB, Li S, Lin S. 2019. Engineering
954 vascularized skeletal muscle tissue with transcriptional factor ETV2-induced autologous
955 endothelial cells. *Protein Cell* **10**:217–222. doi:10.1007/s13238-018-0542-7
956 Yan H, Guo Y, Zhang P, Zu L, Dong X, Chen L, Tian J, Fan X, Wang N, Wu X, Gao W. 2005.
957 Superior neovascularization and muscle regeneration in ischemic skeletal muscles following
958 VEGF gene transfer by rAAV1 pseudotyped vectors. *Biochem Biophys Res Commun*
959 **336**:287–298. doi: 10.1016/j.bbrc.2005.08.066
960 Young MD, Behjati S. 2020. SoupX removes ambient RNA contamination from droplet-based
961 single-cell RNA sequencing data. *Gigascience* **9**:giaa151. doi: 10.1093/gigascience/giaa151.
962 Yue L, Wan R, Luan S, Zeng W, Cheung TH. 2020. Dek Modulates Global Intron Retention

963 during Muscle Stem Cells Quiescence Exit. *Dev Cell* **53**:661-676.e6.
964 doi:10.1016/j.devcel.2020.05.006
965 Zhang MJ, Ntranos V, Tse D. 2020. Determining sequencing depth in a single-cell RNA-seq
966 experiment. *Nat Commun* **11**:1–11. doi:10.1038/s41467-020-14482-y
967 Zheng B, Cao B, Crisan M, Sun B, Li G, Logar A, Yap S, Pollett JB, Drowley L, Cassino T,
968 Gharaibeh B, Deasy BM, Huard J, Péault B. 2007. Prospective identification of myogenic
969 endothelial cells in human skeletal muscle. *Nat Biotechnol* **25**:1025-34. doi:
970 10.1038/nbt1334
971
972

973 **Figure Legends**

974

975 **Figure 1. EC gene signal including VEGF receptor genes in MuSCs.**

976 A) Experimental schema for bulk and single cell sequencing from the
977 *Pax7*$^{CreERT2}$*:R26R*$^{tdT}$*:Flk1*$^{GFP}$ mice. Bulk sequencing performed on MuSCs, ECs and
978 single muscle fibers (SMFs) from uninjured muscle. FACS sorted MuSCs and ECs from
979 uninjured and regenerating TA muscle (3 days following CTX) were run separately on
980 the 10X single cell platform and aggregated.

981 B) Bulk RNAseq showing EC signature in MuSCs. Subset dividing genes that are
982 commonly used to delineate cell identity for MuSCs, ECs and SMFs. Last column shows
983 genes that define macrophages (Mφ), which should not be highly expressed in any on our
984 cell types. Red dots indicate MuSCs, green dots indicate ECs and blue dots indicate
985 SMFs.

986 C) UMAP from aggregated single cell RNAseq shows expression of different phases of
987 MuSCs (quiescent MuSCs, activated MuSCs and myoblasts), ECs (tip ECs and ECs) and
988 from likely contaminant cells such as macrophages (Mφ) and smooth muscle cells
989 (SMC).

990 D) UMAP from aggregated data visualized by sample day showing MuSCs segregated by
991 the sample day but overlap in the EC population. Red dots indicate intact (day 0) and
992 blue dots indicate 3 days following CTX.

993 E) Expression of quality control genes such as *eGFP*, *tdTomato*, *CreERT2* and EC genes
994 such as *Cdh5*, *Kdr* and *Flt1*.

995 F) Genome browser tracks of whole muscle and TU-tagged MuSC nascent RNA
996 (GSE97399, van Velthoven et al., 2017). *Kdr* and *Pecam1* expression can be found in the
997 MuSC fraction. As control, *Myh1* is highly expressed in the whole muscle preparation but
998 largely absent in the MuSC fraction. *Sdc4* and *Calcr* are highly expressed in MuSC and
999 less so in the whole muscle fraction.
1000 G) qPCR for *Kdr, Flt1, Nrp1* and *Nrp2* in EC lines (B.end3 and C166), muscle cell line
1001 (C2C12) and MuSC-derived myoblasts in growth and differentiation medium (DM)
1002 shows low level expression of VEGFRs and VEGF co-receptors.
1003 H) RNAScope of *Flt1* on freshly isolated single muscle fibers from *Pax7*$^{tdT}$ mice shows *Flt1*
1004 expression (green) and tdTomato (red) in MuSCs. Nuclei were counterstained with DAPI
1005 (blue). Scale bar indicates 5 µm.
1006 I) Immunostaining for PECAM1, VE-cadherin (VE-Cad), VEGFA co-receptors (NRP1 and
1007 NRP2) and VEGFA receptors (FLT1 and FLK1) in B.End3 EC cell line and MuSC-
1008 derived myoblasts (MB). Nuclei were counterstained with DAPI (blue). Scale bar
1009 indicates 20 µm.

1010

1011 **Figure 2. VEGFA-FLT1-AKT1 axis controls apoptosis in MuSC *in vitro.***
1012 A) Immunostaining for VEGFA (green) in MuSC-derived myoblasts. Nuclei were
1013 counterstained with DAPI (blue). Scale bar indicates 20 µm.
1014 B) Experimental scheme for assessing apoptosis following thapsigargin induction in
1015 myoblast culture.

1016 C) Decreased cell survival in myoblast *in vitro* as VEGFA is blocked using FLT1-FC (a
1017 VEFGA trap) following thapsigargin induction. This phenotype is partially rescued with
1018 exogenous VEGFA (50 ng/ml).
1019 D) Graphical representation of the VEGF pathway inhibitors used in panel E.
1020 E) Following thapsigargin induction, apoptotic and necrotic cells are increased with
1021 inhibition of FLT1 via FLT1-FC or anti-FLT1 antibody (anti-FLT1 mAb) but not FLK1
1022 (SU5402 and ZM306416) or NRP1-FLK1 inhibition (EG00229) following exogenous
1023 VEGFA (50 ng/ml).
1024 F) 4-OHT induced deletion of *Flt1* in $Pax7^{+/CreER}$:$Flt1^{Loxp/Loxp}$ myoblasts is sufficient to
1025 reduce cell survival in myoblast without induction of apoptosis.
1026 G) Cell survival is decreased *in vitro* in myoblast with thapsigargin induction following 4-
1027 OHT mediated deletion of *Flt1* in $Pax7^{+/CreER}$:$Flt1^{Loxp/Loxp}$ myoblast that is not rescued by
1028 exogenous VEGFA. Blue indicates *MuSC-*$Flt1^{+/+}$, red indicates *MuSC-*$Flt1^{+/+}$ with 50
1029 ng/ml VEGFA, green indicates *MuSC-*$Flt1^{\Delta/\Delta}$ and purple indicates *MuSC-*$Flt1^{\Delta/\Delta}$ with 50
1030 ng/ml VEGFA.
1031 H) Representative images of pAKT (red) in myoblast stained by MyoD (green) in *MuSC-*
1032 $Flt1^{+/+}$ and *MuSC-*$Flt1^{\Delta/\Delta}$ myoblasts induced with exogenous VEGFA. Nuclei were
1033 counterstained with DAPI (blue). Scale bar indicates 50 µm.
1034 I) Quantification of pAKT in myoblasts stained by MyoD in *MuSC-*$Flt1^{+/+}$ and *MuSC-*
1035 $Flt1^{\Delta/\Delta}$ myoblast induced w/wo exogenous VEGFA. VEGFA induction increases pAKT
1036 in *MuSC-*$Flt1^{+/+}$ myoblasts but this response is lost in *MuSC-*$Flt1^{\Delta/\Delta}$ myoblasts.

1037 J) Annexin V quantification of myoblasts transfected with myr-AKT and E4ORF1 to
1038 activate AKT1 showed increased cell survival of myoblasts following thapsigargin
1039 induction.
1040 K) Representative model for VEGFA-FLT1-AKT axis-mediated MuSC survival.
1041

1042 **Figure 3. MuSC-derived *VEGFA* and *Flt1* requires proper skeletal muscle.**

1043 A) Experimental schema detailing the experiments performed in this figure. The
1044 $Pax7^{+/CreER}$:$R26R^{tdT}$:$VEGFA^{+/Hyper}$ ($VEGFA^{+/Hyper}$) $Pax7^{+/CreER}$:$R26R^{tdT}$:$VEGFA^{Loxp/Loxp}$
1045 *for MuSC-*$VEGFA^{\Delta/\Delta}$ and $Pax7^{tdT}$:$Flt1^{Loxp/Loxp}$ for *MuSC-*$Flt1^{\Delta/\Delta}$ lines were pulsed with
1046 tamoxifen (TMX) prior to investigation.
1047 B) Representative H&E-stained images for intact and on 14-day post injury TA muscle from
1048 *MuSC-*$VEGFA^{+/Hyper}$*, MuSC-*$Flt1^{\Delta/\Delta}$ *and MuSC-*$VEGFA^{\Delta/\Delta}$ mice and their representative
1049 controls. Scale bar indicates 50 µm.
1050 C) Annexin V staining show less necrotic cells in MuSC from $VEGFA^{+/Hyper}$ mice compared
1051 with the control one day following injury.
1052 D) Quantification of MuSCs from single muscle fibers show increased MuSCs in
1053 $VEGFA^{+/Hyper}$ EDL muscle compared with the control mice at base line and 14 days post
1054 injury.
1055 E) Fiber size distribution and F) mean feret's diameter of uninjured and regenerating muscle
1056 14 days post injury from $VEGFA^{+/Hyper}$ and control mice show no difference at baseline
1057 but an increase in fiber diameter following injury.
1058 G) Annexin V staining show increased dead cells in MuSCs from *MuSC-*$VEGFA^{\Delta/\Delta}$ mice
1059 one day following CTX compared with the control *MuSC-*$VEGFA^{+/+}$ mice.

1060 H) Quantification of MuSCs from single muscle fiber at base line and 14 days post injury.

1061 I) Fiber size distribution and J) mean feret's diameter of uninjured and regenerating muscle
1062 14 days post injury from *MuSC-VEGFA*$^{\Delta/\Delta}$ and *MuSC-VEGFA*$^{+/+}$ mice show no
1063 difference at baseline but a decrease in fiber diameter following injury.

1064 K) Annexin V staining show increased apoptosis in MuSCs from *MuSC-Flt1*$^{\Delta/\Delta}$ mice one
1065 day following injury compared with the control *MuSC-Flt1*$^{+/+}$ mice.

1066 L) Quantification of MuSCs from single muscle fiber show decreased MuSCs in *MuSC-*
1067 *Flt1*$^{\Delta/\Delta}$ EDL muscle at base line and 14 days post injury compared with the control
1068 *MuSC-Flt1*$^{+/+}$ mice.

1069 M) Fiber size distribution and N) mean feret's diameter of uninjured and regenerating muscle
1070 from *MuSC-Flt1*$^{\Delta/\Delta}$ and compared with the control *MuSC-Flt1*$^{+/+}$ mice show no
1071 difference at baseline but a decrease in fiber diameter following injury.

1072

1073 **Figure 4. VEGFA-FLT1 pathway in MuSCs regulates muscle pathology in DMD model**
1074 **mice.**

1075 A) Experimental schema detailing the experiments performed in this figure. The
1076 *mdx:Pax7*$^{tdT}$*:Flt1*$^{Loxp/Loxp}$ was pulsed with tamoxifen (TMX) to generate *mdx:MuSC-*
1077 *Flt1*$^{\Delta/\Delta}$ mice prior to investigation. *mdx*:*VEGFA*$^{+/Hyper}$ mouse line was used without any
1078 induction.

1079 B) Representative H&E and Sirus red stain from *mdx:MuSC-Flt1*$^{+/+}$ and *mdx:MuSC-Flt1*$^{\Delta/\Delta}$
1080 mouse TA muscle at 3 months of age. Scale bar indicates 50 µm.

1081 C) Smaller average fiber size in *mdx:MuSC-Flt1*$^{\Delta/\Delta}$ compared with the control *mdx:MuSC-*
1082 *Flt1*$^{+/+}$ mouse TA muscle.

1083 D) Increased fibrotic area in *mdx:MuSC-Flt1*$^{\Delta/\Delta}$ compared with the control *mdx:MuSC-*
1084 *Flt1*$^{+/+}$ mouse TA muscle.
1085 E) Decreased muscle perfusion in *mdx:MuSC-Flt1*$^{\Delta/\Delta}$ compared with the control *mdx:MuSC-*
1086 *Flt1*$^{+/+}$ mouse TA muscle.
1087 F) Decreased grip strength normalized to body weight in *mdx:MuSC-Flt1*$^{\Delta/\Delta}$ compared with
1088 the control *mdx:MuSC-Flt1*$^{+/+}$ mouse TA muscle at both 3 and 12 months of age.
1089 G) Representative H&E and Sirus red stain from *mdx*:*VEGFA*$^{+/Hyper}$ and *mdx*:*VEGFA*$^{+/+}$
1090 mouse TA muscle at 3 months from TA muscle (top four panels) and diaphragm muscle
1091 (bottom four panels).
1092 H) Increased average fiber size in *mdx*:*VEGFA*$^{+/Hyper}$ compared with the control
1093 *mdx*:*VEGFA*$^{+/+}$ mouse TA and diaphragm (DM) muscle. Scale bar indicates 50 µm.
1094 I) Decreased fibrosis in *mdx*:*VEGFA*$^{+/Hyper}$ compared with the control *mdx*:*VEGFA*$^{+/+}$
1095 mouse TA muscle.
1096 J) Decreased fibrosis in *mdx*:*VEGFA*$^{+/Hyper}$ compared with the control *mdx*:*VEGFA*$^{+/+}$
1097 mouse diaphragm (DM) muscle.
1098 K) Muscle perfusion is increased in *mdx*:*VEGFA*$^{+/Hyper}$ compared with the control
1099 *mdx*:*VEGFA*$^{+/+}$ mouse TA muscle.
1100 L) Grip strength normalized to body weight is increased in *mdx*:*VEGFA*$^{+/Hyper}$ compared
1101 with the control *mdx*:*VEGFA*$^{+/+}$ mice.

# Figure 1

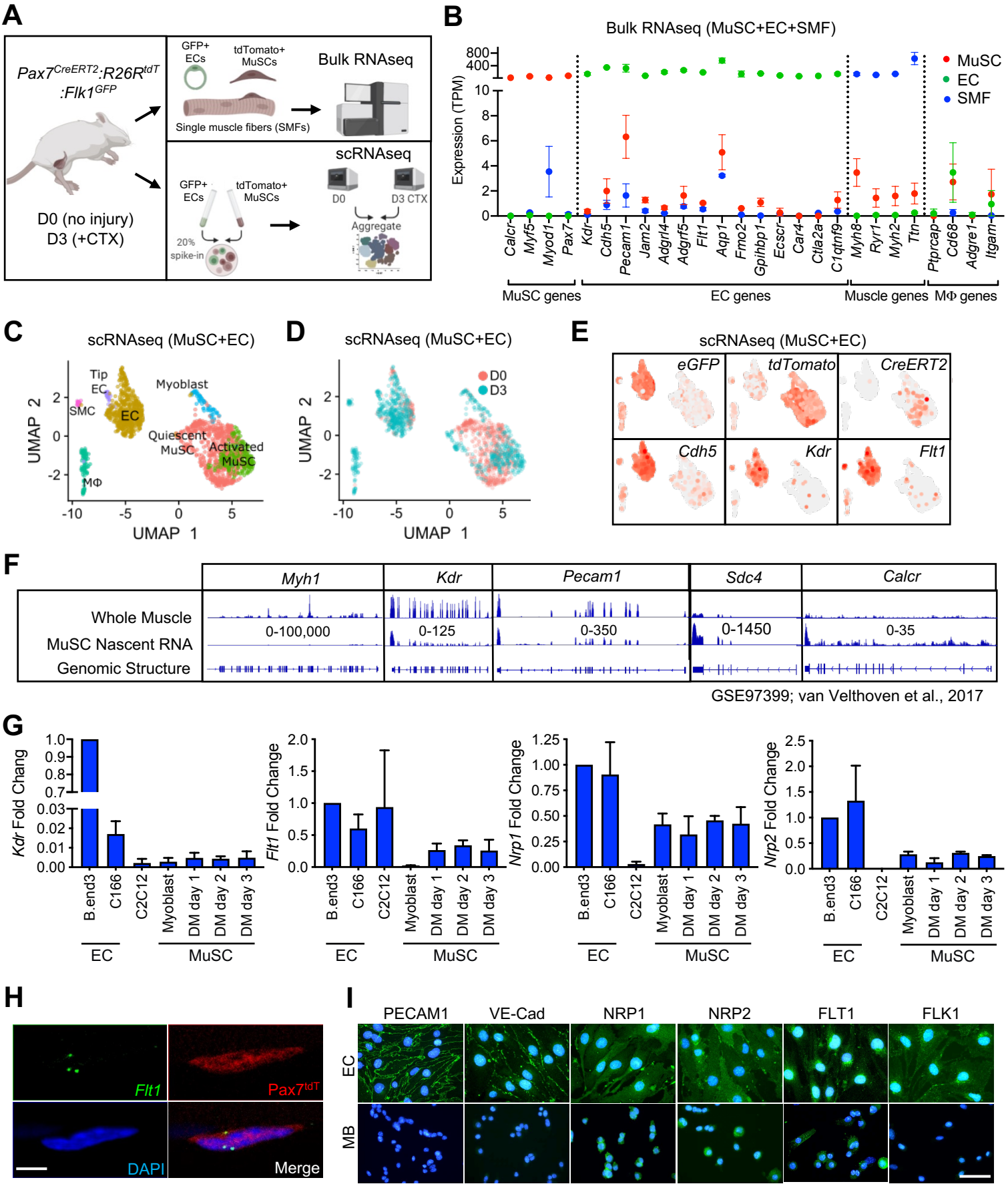
A
Pax7CreERT2:R26RtdT:Flk1GFP
D0 (no injury)
D3 (+CTX)
GFP+ ECs
tdTomato+ MuSCs
Single muscle fibers (SMFs)
Bulk RNAseq
scRNAseq
D0
D3 CTX
Aggregate
20% spike-in
B
Bulk RNAseq (MuSC+EC+SMF)
Expression (TPM)
MuSC
EC
SMF
Calcr Myf5 Myod1 Pax7 Kdr Cdh5 Pecam1 Jam2 Adgrl4 Adgrf5 Flt1 Aqp1 Fmo2 Gpihbp1 Ecscr Car4 Ctla2a C1qtnf9 Myh8 Ryr1 Myh2 Ttn Ptprcap Cd68 Adgre1 Itgam
MuSC genes
EC genes
Muscle genes
MΦ genes
C
scRNAseq (MuSC+EC)
Tip EC
SMC
EC
Myoblast
Quiescent MuSC
Activated MuSC
MΦ
UMAP 2
UMAP 1
D
scRNAseq (MuSC+EC)
D0
D3
UMAP 2
UMAP 1
E
scRNAseq (MuSC+EC)
eGFP
tdTomato
CreERT2
Cdh5
Kdr
Flt1
F
Myh1
Kdr
Pecam1
Sdc4
Calcr
Whole Muscle
MuSC Nascent RNA
Genomic Structure
0-100,000
0-125
0-350
0-1450
0-35
GSE97399; van Velthoven et al., 2017
G
Kdr Fold Chang
Flt1 Fold Change
Nrp1 Fold Change
Nrp2 Fold Change
B.end3
C166
C2C12
Myoblast
DM day 1
DM day 2
DM day 3
EC
MuSC
H
Flt1
Pax7tdT
DAPI
Merge
I
PECAM1
VE-Cad
NRP1
NRP2
FLT1
FLK1
EC
MB

# Figure 2

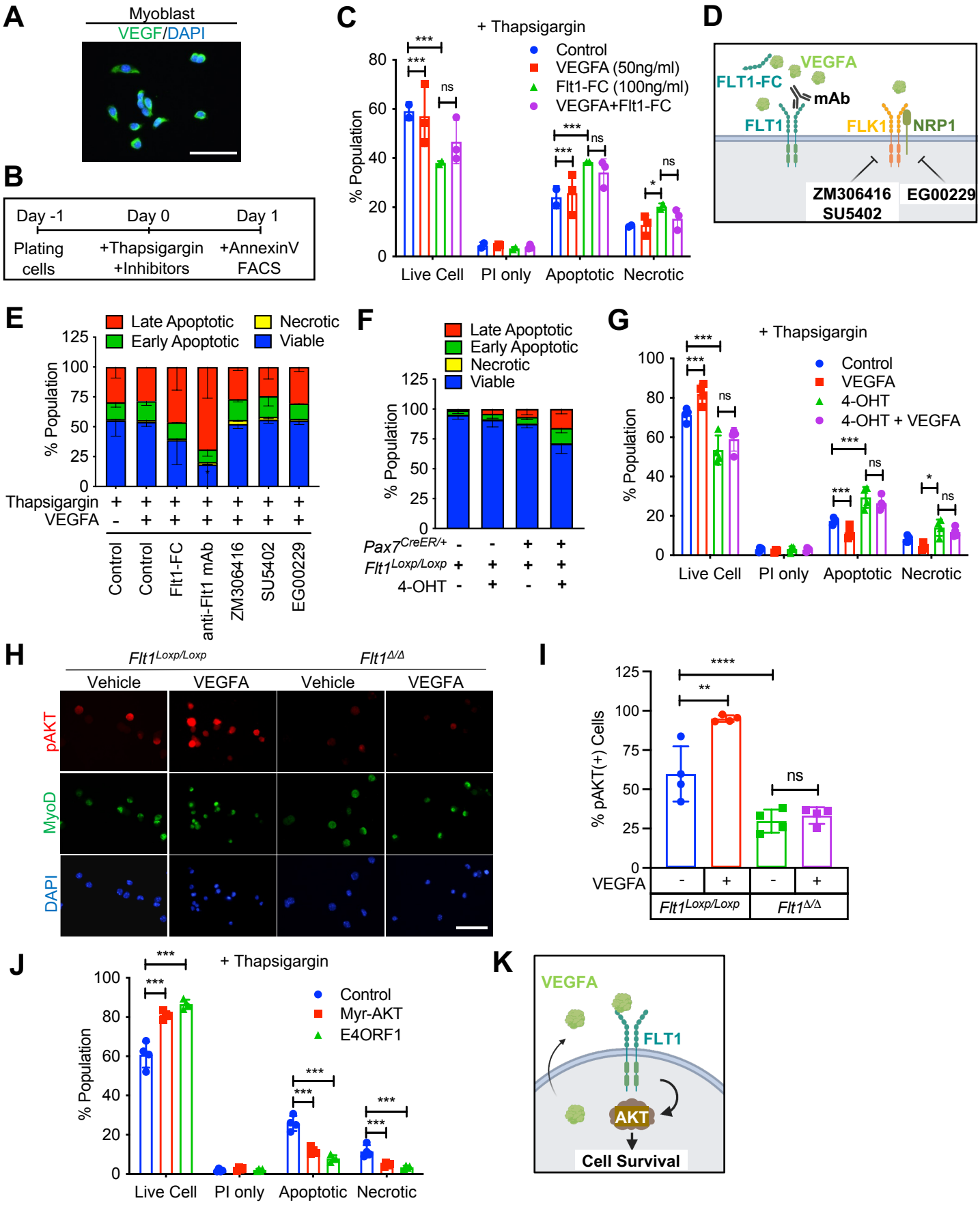
A
Myoblast
VEGF/DAPI
B
Day -1
Day 0
Day 1
Plating cells
+Thapsigargin +Inhibitors
+AnnexinV FACS
C
+ Thapsigargin
Control
VEGFA (50ng/ml)
Flt1-FC (100ng/ml)
VEGFA+Flt1-FC
% Population
Live Cell
PI only
Apoptotic
Necrotic
D
VEGFA
FLT1-FC
mAb
FLT1
FLK1
NRP1
ZM306416
SU5402
EG00229
E
Late Apoptotic
Early Apoptotic
Necrotic
Viable
% Population
Thapsigargin
VEGFA
Control
Control
Flt1-FC
anti-Flt1 mAb
ZM306416
SU5402
EG00229
F
Late Apoptotic
Early Apoptotic
Necrotic
Viable
% Population
Pax7CreER/+
Flt1Loxp/Loxp
4-OHT
G
+ Thapsigargin
Control
VEGFA
4-OHT
4-OHT + VEGFA
% Population
Live Cell
PI only
Apoptotic
Necrotic
H
Flt1Loxp/Loxp
Flt1Δ/Δ
Vehicle
VEGFA
Vehicle
VEGFA
pAKT
MyoD
DAPI
I
% pAKT(+) Cells
VEGFA
Flt1Loxp/Loxp
Flt1Δ/Δ
J
+ Thapsigargin
Control
Myr-AKT
E4ORF1
% Population
Live Cell
PI only
Apoptotic
Necrotic
K
VEGFA
FLT1
AKT
Cell Survival

# Figure 3

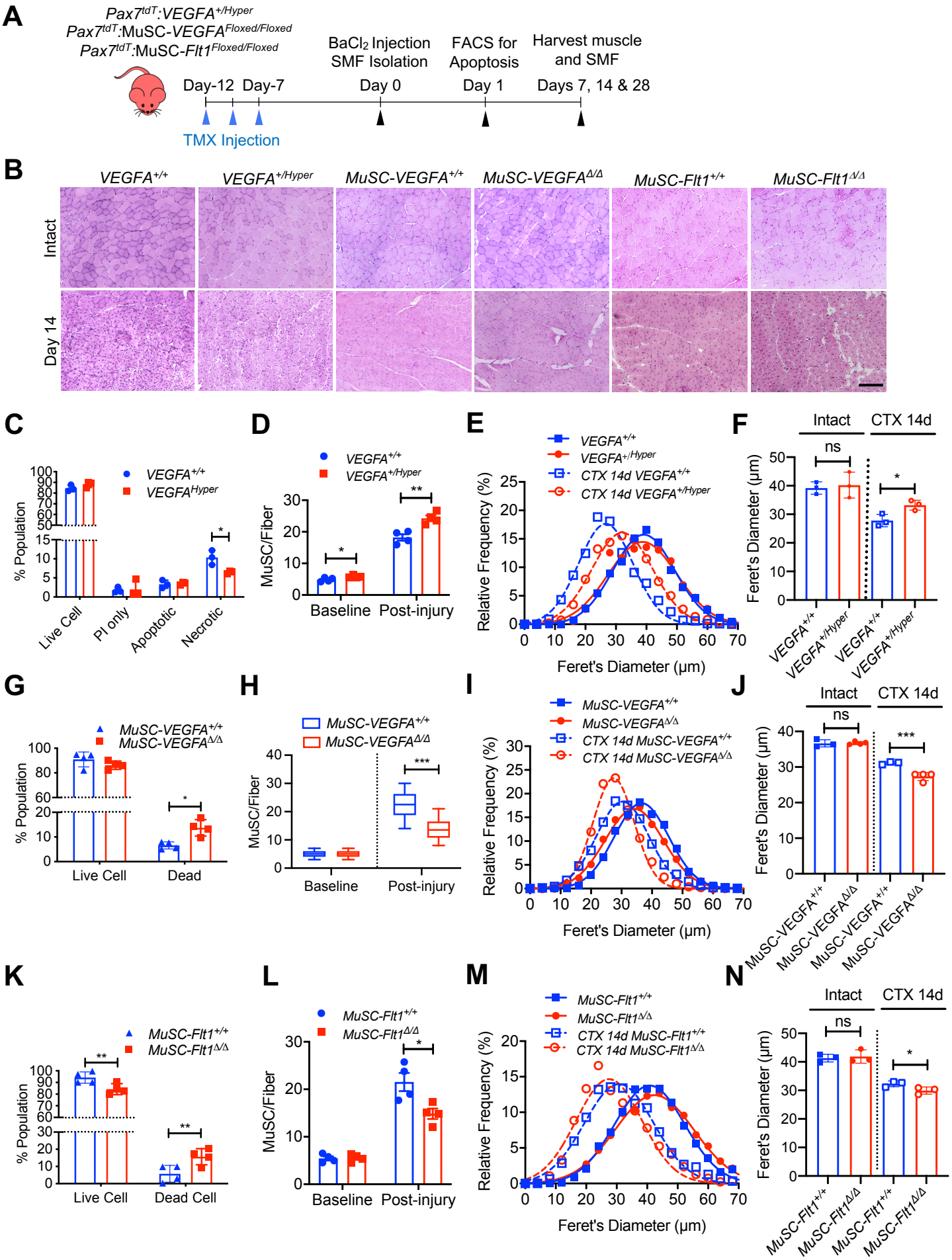
A
Pax7tdT:VEGFA+/Hyper
Pax7tdT:MuSC-VEGFAFloxed/Floxed
Pax7tdT:MuSC-Flt1Floxed/Floxed
BaCl2 Injection
SMF Isolation
FACS for Apoptosis
Harvest muscle and SMF
Day-12 Day-7
Day 0
Day 1
Days 7, 14 & 28
TMX Injection
B
VEGFA+/+
VEGFA+/Hyper
MuSC-VEGFA+/+
MuSC-VEGFAΔ/Δ
MuSC-Flt1+/+
MuSC-Flt1Δ/Δ
Intact
Day 14
C
% Population
VEGFA+/+
VEGFAHyper
Live Cell
PI only
Apoptotic
Necrotic
D
MuSC/Fiber
Baseline
Post-injury
E
Relative Frequency (%)
CTX 14d VEGFA+/+
CTX 14d VEGFA+/Hyper
Feret's Diameter (µm)
F
Intact
CTX 14d
ns
Feret's Diameter (µm)
G
MuSC-VEGFA+/+
MuSC-VEGFAΔ/Δ
Live Cell
Dead
H
I
CTX 14d MuSC-VEGFA+/+
CTX 14d MuSC-VEGFAΔ/Δ
J
K
MuSC-Flt1+/+
MuSC-Flt1Δ/Δ
Dead Cell
L
M
CTX 14d MuSC-Flt1+/+
CTX 14d MuSC-Flt1Δ/Δ
N

# Figure 4

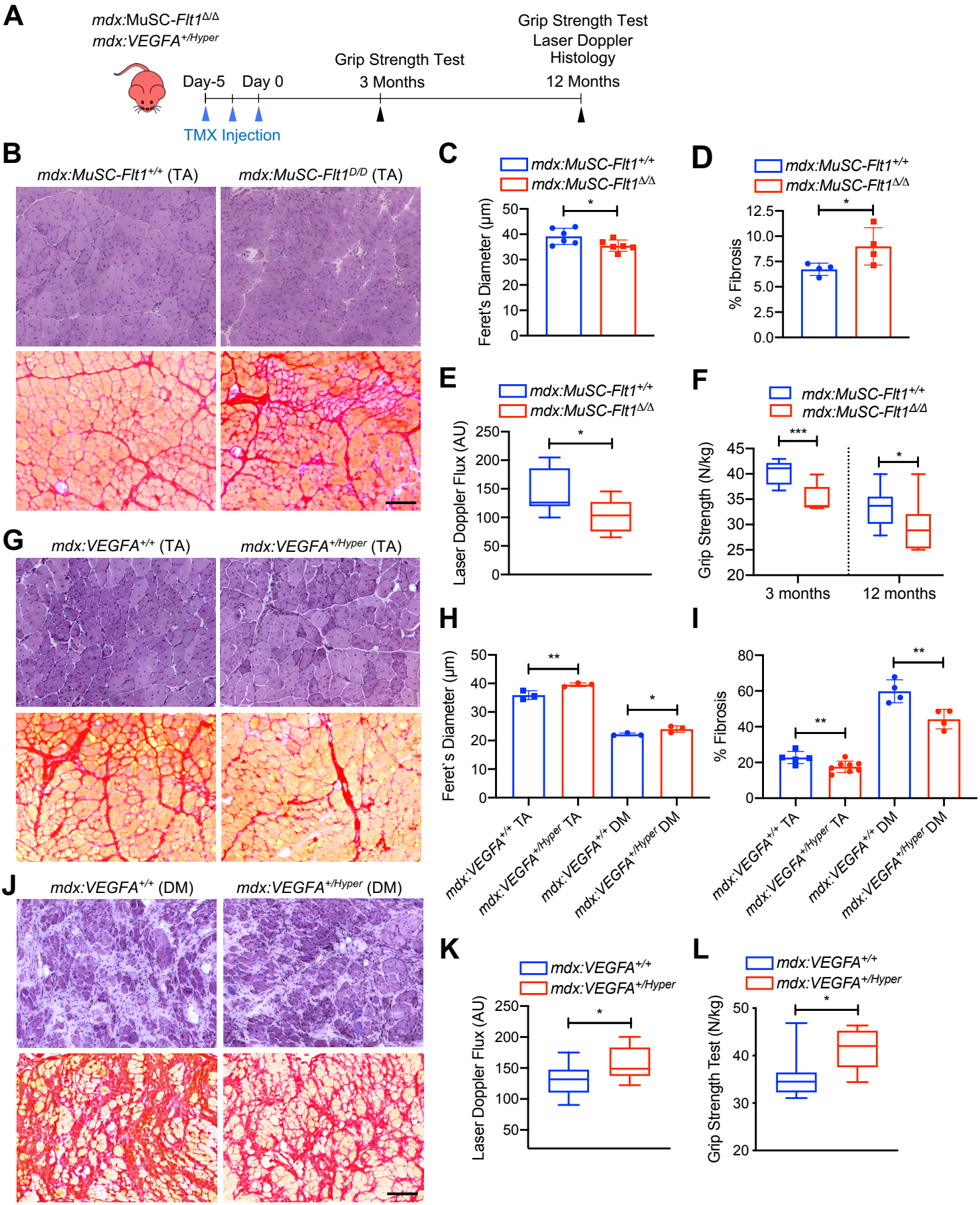
A
mdx:MuSC-Flt1Δ/Δ
mdx:VEGFA+/Hyper
Day-5
Day 0
TMX Injection
Grip Strength Test
3 Months
Grip Strength Test
Laser Doppler
Histology
12 Months
B
mdx:MuSC-Flt1+/+ (TA)
mdx:MuSC-Flt1D/D (TA)
C
mdx:MuSC-Flt1+/+
mdx:MuSC-Flt1Δ/Δ
Feret's Diameter (µm)
D
% Fibrosis
E
Laser Doppler Flux (AU)
F
Grip Strength (N/kg)
3 months
12 months
G
mdx:VEGFA+/+ (TA)
mdx:VEGFA+/Hyper (TA)
H
Feret's Diameter (µm)
mdx:VEGFA+/+ TA
mdx:VEGFA+/Hyper TA
mdx:VEGFA+/+ DM
mdx:VEGFA+/Hyper DM
I
% Fibrosis
J
mdx:VEGFA+/+ (DM)
mdx:VEGFA+/Hyper (DM)
K
mdx:VEGFA+/+
mdx:VEGFA+/Hyper
Laser Doppler Flux (AU)
L
Grip Strength Test (N/kg)